Geosci. Model Dev. Discuss., 6, 4603–4663, 2013
www.geosci-model-dev-discuss.net/6/4603/2013/
doi:10.5194/gmdd-6-4603-2013

Geoscientific Model Development Discussions
Open Access

Effects of vegetation structure on biomass accumulation in a Balanced Optimality Structure Vegetation Model (BOSVM v1.0)

Z. Yin[1], S. C. Dekker[2], B. J. J. M. van den Hurk[1,3], and H. A. Dijkstra[1]

[1]Institute for Marine and Atmospheric research Utrecht, Utrecht University, Utrecht, the Netherlands
[2]Copernicus Institute of Sustainable Development, Utrecht University, Utrecht, the Netherlands
[3]Royal Netherlands Meteorological Institute, De Bilt, the Netherlands

Received: 18 July 2013 – Accepted: 19 August 2013 – Published: 9 September 2013

Correspondence to: Z. Yin (z.yin@uu.nl)

Published by Copernicus Publications on behalf of the European Geosciences Union.

Abstract

A myriad of interactions exist between vegetation and local climate for arid and semi-arid regions. Vegetation function, structure and individual behavior have large impacts on carbon-water-energy balances, which consequently influence local climate variability that, in turn, feeds back to the vegetation. In this study, a conceptual vegetation structure scheme is formulated and tested in a new carbon-water-energy coupled model to explore the importance of vegetation structure and vegetation adaptation to water stress on equilibrium biomass states. Surface energy, water and carbon fluxes are simulated for a range of vegetation structures across a precipitation gradient in West Africa and optimal vegetation structures that maximizes biomass for each precipitation regime are determined. Two different strategies of vegetation adaptation to water stress are included. Under dry conditions vegetation tries to maximize the Water Use Efficiency and Leaf Area Index as it tries to maximize carbon gain. However, an important negative feedback mechanism is found as the vegetation also tries to minimize its cover to optimize the surrounding bare ground area from which water can be extracted, thereby forming patches of vertical vegetation. Under larger precipitation, a positive feedback mechanism is found in which vegetation tries to maximize its cover as it then can reduce water loss from bare soil while having maximum carbon gain due to a large Leaf Area Index. The competition between vegetation and bare soil determines a transition between a "survival" state to a "growing" state.

1 Introduction

Vegetation has a significant impact on the regional climate at different spatial and temporal scales through interactions with the atmosphere, the hydrological cycle and the surface energy balance (Bonan, 2008; Dekker et al., 2010). Positive and negative vegetation-climate feedbacks can affect the local climate variability particularly in arid and semi-arid regions owing to the complex vegetation-atmosphere interactions

GMDD
6, 4603–4663, 2013

and strong gradients in climate regimes (Entekhabi et al., 1992; Dekker et al., 2007; Seneviratne et al., 2010; Koster et al., 2004). Vegetation feedbacks mitigate surface warming by transpiration, but simultaneously can increase the surface energy absorption by reduction of the surface albedo, affecting the resilience to drought (Teuling et al., 2010; Bonan, 2008).

For arid and semi-arid areas, the strong gradients and spatial variability of vegetation cover (Sankaran et al., 2005; Dijkstra, 2011) and the gross complexity of interactions between vegetation, precipitation (Higgins et al., 2010; Baudena et al., 2010) and bare soil (Rietkerk et al., 2002; Seneviratne et al., 2010; Koster et al., 2004; Zeng et al., 1999) introduce a large range of equilibrium states. An adequate representation of the regimes of interaction between vegetation and climate is necessary to understand the role of vegetation in the climate system, including the ecosystem response to climate change. For this, an enhanced knowledge of soil moisture-vegetation-atmosphere interactions and feedbacks at multiple spatial and temporal scales is needed (Seneviratne et al., 2010; Kéfi et al., 2007; Dijkstra, 2011; Rietkerk et al., 2011).

In arid and semi-arid areas, water availability is a primary factor for photosynthesis and vegetation development (Seneviratne et al., 2010). In a model experiment, Koster et al. (2004) revealed that soil moisture and precipitation are strongly coupled in water transition zones including the Western Africa monsoon area. This strong interaction points at a potentially strong role of vegetation-climate interactions in this region. Observations show a good correspondence between maximum vegetation cover and annual mean precipitation (Sankaran et al., 2005; Guan et al., 2012; Hirota et al., 2011). However, for a given precipitation amount the observed cover fraction of woody vegetation varies significantly. One factor that may play a role here is the vegetation response to fire (Sankaran et al., 2005; Higgins et al., 2010; Hirota et al., 2011; Staver et al., 2011), which will lead to a fast replacement of woody vegetation by grass. This can explain the strong variability of woody vegetation cover in so-called “alternative stable states” (Hirota et al., 2011). Baudena et al. (2010) showed how the co-existent regimes of tree and grass species depend on the chosen parameterization options in

GMDD
6, 4603–4663, 2013

their conceptual model, pointing at the need for a detailed understanding of the underlying biophysical processes.

Recently, many studies focus on how precipitation influences vegetation patterns through processes of water re-distribution, such as positive feedbacks due to infiltration (Rietkerk et al., 2002), shading (Baudena and Provenzale, 2008) and topography (Klausmeier, 1999). In these studies transpiration, which is the crucial process in water, carbon and energy balances, is not explicitly modeled. In these conceptual models, transpiration rate simply has a positive relation with biomass density, vegetation fraction or soil water stress. However, the ability of these conceptual models to describe vegetation dynamics and feedbacks to specific climate is generally limited by their degree to which mechanistic processes are included and energy or mass balance closure is satisfied. In addition, different vegetation strategies of vegetation response to drought (Calvet, 2000; Calvet et al., 2004) will also influence vegetation fraction and biomass significantly. On the other hand, these conceptual models are tested under simulated precipitation gradient. In fact, across the precipitation gradient, also other climate variables (radiation, air humidity, wind speed, etc) varies and influences vegetation processes.

In the interaction between vegetation and the coupled water-carbon-energy balance, spatial structure of vegetation plays an important role to transpiration on multiple time scales (e.g. Konings et al., 2011). Within a given set of climate conditions, a large variation of water uptake ability and CO_2 assimilation rate exists, controlled by vegetation structure characteristics such as root biomass, Leaf Area Index (LAI) and leaf cover (f_c). LAI affects the potential transpiration rate of a plant and it changes the surface albedo, which controls the absorption of solar energy by the land surface. f_c plays a key role in the vegetation-bare soil competition for water and energy. In water limited regimes, bare ground evaporation will reduce the available water needed for photosynthesis, directly affecting biomass accumulation. In addition, the shoot-root distribution of vegetation determines the balance between water uptake and carbon gain.

GMDD
6, 4603–4663, 2013

Both LAI and f_c increase as biomass is accumulated. However, for a given leaf biomass, spatially different vegetation structures can be generated. High LAI/f_c values imply an ecosystem developing a vertical structure (e.g. individual trees or patches of dense grass), while low LAI/f_c is representative for horizontally oriented vegetation structures (e.g. grassland or rainforest).

Simultaneously, different strategies exist on regulating stomata response to water stress. Calvet (2000) and Calvet et al. (2004) identified two distinct strategies (drought avoiding or drought tolerant), which affects the response of vegetation to shorter or longer dry periods. Drought tolerant ("offensive") species tend to maximize water use in dry conditions, rapidly making benefit of precipitation events in a dry climate. Drought avoiding ("defensive") strategies lead to a more conservative response to moisture anomalies, aiming at preserving water for times of scarcity.

In this study, our first aim is to investigate how vegetation adjusts to climate by optimizing its spatial structure. We explore the impact of vegetation structure and drought strategies on the equilibrium vegetation biomass for a strong gradient in climate conditions found in the West African Sahel area. Climate forcing data are from observations (Boone et al., 2009). Effects of the chosen strategies on vegetation functions, such as maximum Water Use Efficiency or total biomass (Schymanski et al., 2008, 2010) are analyzed. In our study we assume that the main aim of vegetation structure optimization is to produce maximum total biomass (Schymanski et al., 2010), while others have tried to maximize net carbon profit (Schymanski et al., 2007; Dekker et al., 2012) or minimize soil water stress (Rodriguez-Iturbe et al., 1999). Through the optimization process, we will simulate how optimal vegetation structure shifts with climate change by carbon allocation and strategies to drought, which is the second aim of this study. By understanding the mechanism that leads to the shift of the optimal structure , we can enhance the prediction of phenology change with climate.

A new coupled carbon-water-energy balance model simulating biomass dynamics is developed from existing model components. Vegetation structure parameterization follows LPJ (Sitch et al., 2003) and TRIFFID (Cox, 2001). Photosynthesis and canopy

GMDD
6, 4603–4663, 2013

conductance simulation are based on CTESSEL (Boussetta et al., 2013) and Calvet (2000); Calvet et al. (2004). Energy and water balances are calculated as formulated in TESSEL (van den Hurk et al., 2000; Balsamo et al., 2009). Monin-Obkhov similarity theory (Oleson et al., 2004; ECMWF, 2008) is applied for estimation of aerodynamic exchange. We make use of existing concepts of current ecological and hydrometeorological models, but configured with sufficient flexibility to explore a range of relevant features related to the vegetation structure, competition with bare ground evaporation, and light absorption. The model includes the main physical and biological land surface processes coupling the cycles of carbon, water and energy. The definition of the vegetation structure in this model is conceptualized in order to represent spatial structures of vegetation in different Plant Function Types (PFTs). Competition between bare soil and vegetation is included by using a tiling method (van den Hurk et al., 2000). In a next study, we will try to enhance our knowledge of the role vegetation plays in land-atmosphere interactions. The new model developed in this study can be easily combined with existing climate models for future land-atmosphere interaction studies.

2 Methodology: model description and experimental design

The primary aspect of our model is the combination of water, carbon, and energy balances. During the closing of these three balances, surface conductance (g_s) plays a crucial role, which is influenced by numerous climate variables. In stead of using an empirical stress formulation of the Jarvis approach (Jarvis, 1976), we first simulate vegetation photosynthesis activity, which highly depends on both vegetation behavior and climate condition. From photosynthesis simulation, we retrieve surface conductance and use it in Monin-Obukohv similarity theory to estimate aerodynamic conductance (g_a). After g_s and g_a are known, we can estimate sensible and latent heat flux by closing the surface energy balance. States of surface temperature, soil water and total biomass will be updated. Based on specific vegetation structure parameters (α and D)

GMDD
6, 4603–4663, 2013

and updated biomass, we can calculate LAI, vegetation cover and root density in the next time step.

Section 2.1 introduces the fundamental equations of the energy, water and carbon balance. Section 2.2 illustrates the definitions of vegetation structures and formulation of structure variables (LAI, f_c and root density). In Sects. 2.3, 2.4 and 2.5, detailed parameterization of terms in carbon, energy and water balance equations (in Sect. 2.1) are displayed, respectively. Section 2.6 introduces two vegetation strategies to water stress found by Calvet (2000) and Calvet et al. (2004). In addition, we illustrate corresponding intrinsic water use efficiency as a function of extractable soil water content. In Sect. 2.7, we discuss how vegetation structure parameters effect biomass via LAI, f_c and root density. Sections 2.8 and 2.9 show the details of simulation process and information of study area, respectively.

2.1 Model concepts

Our model is designed to describe the coupled dynamics of the budgets of surface energy, water and carbon. Each budget is governed by a balance equation given by,

$$R_n = H + lE + G \tag{1}$$

$$\frac{dW}{dt} = (P - \text{Leak} - E)C\,A_{ref} \tag{2}$$

$$\frac{dC_{veg}}{dt} = NPP \cdot CA - LIT \tag{3}$$

where the budgets for water and energy are expressed as mass or energy per unit crown area. R_n [$W\,m^{-2}$] is net radiation; H [$W\,m^{-2}$] is sensible heat flux; lE [$W\,m^{-2}$] is latent heat flux and G [$W\,m^{-2}$] is soil heat flux; W [$kg\,H_2O$] is total water stored

GMDD
6, 4603–4663, 2013

in the soil; P [kg H_2O m^{-2} s^{-1}] is the precipitation rate; Leak [kg H_2O m^{-2} s^{-1}] is water leakage through bottom drainage; E [kg H_2O m^{-2} s^{-1}] is evapotranspiration rate; CA_{ref} [m^2] is the reference crown area, identical to the maximum size of an individual plant; t [s] is time step of the simulation; C_{veg} [kg C] is the total amount of biomass; NPP [kg C m^{-2} s^{-1}] is net primary production; CA [m^2] is crown area of vegetation; LIT [kg C s^{-1}] is generation of litter of vegetation.

2.2 Carbon allocation and canopy structure

The vegetation carbon biomass pool is distributed over above ground and below ground components. In our model vegetation is separated into two classes: grass, for which the above ground carbon pool exists of leaf biomass only, and woody plants, for which the above ground biomass is composed of leaf biomass and stem biomass to support a high LAI (see top left panel of Fig. 1). The biomass composition function is therefore,

$$C_{veg} = C_{leaf} + C_{root} + C_{stem} \tag{4}$$

where C_{leaf} [kg C] is leaf biomass; C_{root} [kg C] is root biomass; C_{stem} [kg C] is stem biomass (zero for grass, see Fig. 1).

The shoot-root ratio α[-], defined by,

$$\alpha = \frac{C_{leaf} + C_{stem}}{C_{veg}} \tag{5}$$

α is our first control parameter. A high value of α implies more biomass to be allocated to leaves, enhancing the potential carbon assimilation rate, while a low α implies higher water uptake abilities due to higher root density (see top right panel of Fig. 1). Observed values of α range between 0 and 0.5 (Sitch et al., 2003).

GMDD
6, 4603–4663, 2013

For the allocation of stem biomass in woody vegetation, we use the expression from the TRIFFID model (Cox, 2001), reading,

$$\frac{C_{\text{stem}}}{\text{CA}} = a_l \cdot \text{LAI}^{5/3} \tag{6}$$

where a_l is a PFT-dependent parameter (see Table 1 for an overview of parameters used).

We calculate LAI following the global dynamic vegetation model LPJ (Sitch et al., 2003) using a predefined value of the Specific Leaf Area (SLA), ignoring possible variation with leaf age or nitrogen content.

$$\text{LAI} = \frac{C_{\text{leaf}} \cdot \text{SLA}}{\text{CA}} \tag{7}$$

where SLA [$\text{m}^2\,\text{kgC}^{-1}$] is a constant (Table 3). For a given value of C_{leaf}, CA is inversely proportional to LAI.

The second control parameter, representing the trade-off between CA and LAI, is the ratio between relative CA and relative LAI (Eq. 8). The control parameter D governs this ratio, using a scaling value LAI_{ref} as a constant (Table 3).

$$D = \frac{\text{LAI}}{\text{LAI}_{\text{ref}}} \Big/ \frac{\text{CA}}{\text{CA}_{\text{ref}}} \tag{8}$$

A high value of D implies a vegetation canopy that has a vertical orientation, while a low D means a horizontal structure (top right panel of Fig. 1). For a realistic description of real canopies D is varied in the range between 0.1 and 5.

Vegetation fraction f_c is the ratio of projected leaf area to the reference crown area (bottom left panel of Fig. 1), which can be calculated by:

$$f_c = f_s \left(1 - e^{-k \cdot \text{LAI}}\right) \tag{9}$$

GMDD
6, 4603–4663, 2013

where $f_s = \mathrm{CA}/\mathrm{CA}_{\mathrm{ref}}$[-] is the relative crown area; k [-] is a constant extinction factor.

For values of CA close to $\mathrm{CA}_{\mathrm{ref}}$ and relatively low values of LAI, f_c and LAI are positively related. For $f_s = 1$, the crown area cannot increase anymore, and additional leaf biomass will result in a LAI increase, even when this would imply $\mathrm{LAI} > \mathrm{LAI}_{\mathrm{ref}}$. Notice that in this case, the canopy structure changes due to the constant CA and the increasing LAI.

The crown area CA is also used to define a root density φ [kg C m^{-2}], assuming an equal distribution of root biomass over the crown area according to,

$$\varphi = \frac{C_{\mathrm{root}}}{\mathrm{CA}} \tag{10}$$

which is used to calculate the extractable soil water fraction. Furthermore, it influences the opening of stomata and the surface conductivity (more details in Sect. 2.6 and Appendix B).

2.3 Model formulation of biomass dynamics and NPP

The total biomass change is controlled by carbon gain from Net Primary Production (NPP) and carbon loss by litter fall (Eq. 3). NPP is equal to gross primary production (GPP) minus dark respiration (R_{d}). GPP is governed by the photosynthetic uptake of carbon, modeled following of the ISBA-A-g_{s} model (Jacobs et al., 1996; Calvet, 2000; Calvet et al., 2004) (see Appendix B for a full description of the photosynthesis model).

LIT is parameterized using an exponential decay of the actual biomass using a predefined residence time due to litter decomposition, which is longer for woody plants than for grass (Table 1).

$$\mathrm{LIT} = \frac{C_{\mathrm{leaf}}}{\tau_{\mathrm{leaf}}} + \frac{C_{\mathrm{stem}}}{\tau_{\mathrm{stem}}} + \frac{C_{\mathrm{root}}}{\tau_{\mathrm{root}}} \tag{11}$$

where τ_{leaf}, τ_{stem} and τ_{root} [s] are residence time due to litter decomposition of leaf, stem and root respectively (Table 1).

GMDD
6, 4603–4663, 2013

As indicated before, N P P is allocated over root, stem and leaf biomass. Three common approaches for N P P allocation exist (Malhi et al., 2011). The simplest way is to use fixed allocation fractions for each carbon pool. Due to different decay time scales for leaf and root (Table 1), the shoot-root ratio α will vary over time as a consequence of this, which is not desirable for our purpose. Another approach assumes that N P P allocation is influenced by the availability of resources. For instance, more N P P is allocated to roots under conditions of water and nutrients scarcity, while more N P P is allocated to leaves in light limited conditions. The method that we used follows LPJ and TRIFFID (Sitch et al., 2003; Cox, 2001), which simulate allocation of N P P by allometric constraints.

Photosynthesis is complex as it is not only determined by environmental elements, but also by the vegetation response to the change of environment. In the A-g_s model, the photosynthetic rate is limited by surface temperature, CO_2 concentration, water vapor deficit, incoming solar radiation, and available soil moisture (Calvet, 2000; Calvet et al., 2004). In our model we specify an effective extractable soil water fraction f_w as function of soil moisture content and variable root density following,

$$f_w = \frac{\theta_2 - \theta_{pwp}}{\theta_{cap} - \theta_{pwp}} \cdot \frac{\varphi}{\varphi_{max}} \tag{12}$$

where θ_2 [$m^3\,m^{-3}$] is volumetric soil moisture content in the root layer (second layer, see bottom right panel of Fig. 1); θ_{pwp}, and θ_{cap} [$m^3\,m^{-3}$] are (fixed) soil moisture at wilting point, field capacity respectively; φ_{max} is the root density leading to the maximum water uptake ability of plants (Table 1). Available water is thus explicitly dependent on the amount of root biomass.

2.4 The surface energy balance and geometric structure of model

In our model the energy balance is explicitly simulated for two distinct surface fractions (tiles): a bare ground and a vegetation tile (see bottom right panel of Fig. 1). Vegetation

GMDD
6, 4603–4663, 2013

can utilize deep soil water for evapotranspiration, while bare soil has access to a much shallower water reservoir. For this reason we applied a two soil layer scheme. The depth of the first and second layer is 0.02 and 0.48 m respectively. Bare soil only can use water from the top layer while vegetation uses the water from the second layer.

Equation 1 can be rewritten for both vegetation and bare soil tiles:

$$R_{n,[v;b]} = H_{[v;b]} + l E_{[v;b]} + G_{[v;b]} \quad (13)$$

Subscript "v" is used for terms that apply to the vegetation tile, while subscript "b" is used for the bare ground tile.

Net radiation $R_{n,[v;b]}$ is given as

$$R_{n,[v;b]} = (1 - a_{[v;b]}) \cdot R_{swd} + \epsilon \cdot R_{lwd} - \epsilon \cdot \sigma \cdot T^4_{s,[v;b]} \quad (14)$$

where $T_{s,[v;b]}$ [K] is surface temperature; $a_{[v;b]}$ [-] is surface albedo. For bare ground, a_b [-] is a constant (0.4), while a_v depends on LAI as,

$$a_v = a_{min} + (a_{max} - a_{min}) \cdot e^{-k \cdot LAI} \quad (15)$$

where $a_{min} = 0.1$ [-] and $a_{max} = 0.4$ [-].

Latent heat flux ($l E_{[v;b]}$) is given by,

$$l E_{[v;b]} = l \rho_a \frac{q_s(T_{s,[v;b]}) - q_a}{1/g_a + 1/g_{s,[v;b]}} \quad (16)$$

where l [J kg H_2O^{-1}] is latent heat of vaporization, ρ_a [kg m^{-3}] is air density at constant pressure, g_a [m s^{-1}] is aerodynamic conductance, $g_{s,[v;b]}$ [m s^{-1}] is surface conductance, q_s [Pa] is surfaced saturated specific humidity, q_a [Pa] is air specific humidity.

For vegetation, $g_{s,v}$ is equal to the canopy conductance (see Appendix B), while for bare ground $g_{s,b}$ is given by,

$$g_{s,b} = g_{s,max} \cdot f^*_w \quad (17)$$

GMDD
6, 4603–4663, 2013

where $g_{s,max}$ [m s^{-1}] is the maximum surface conductance of bare soil; f_w^* [-] is extractable water factor of bare ground given by,

$$f_w^* = \frac{\theta_1 - \theta_r}{\theta_{cap} - \theta_r} \tag{18}$$

where θ_1 [m^3 m^{-3}] is soil moisture from the top soil layer (first layer), $\theta_r = 0.01$ [m^3 m^{-3}] is residual soil moisture.

Sensible heat flux is calculated as

$$H_{[v;b]} = \rho_a c_p g_a \left(T_{s,[v;b]} - T_a\right) \tag{19}$$

where c_p [J kg^{-1} K^{-1}] is specific heat capacity of air; T_a [K] is air temperature at 2 m.

The soil heat flux is defined as

$$G_{[v;b]} = -2C_1 \frac{T_1 - T_{s,[v;b]}}{z_1} \tag{20}$$

where C_1 [W m^{-1} K^{-1}] is thermal conductivity of the soil; T_1 [K] is soil the temperature of the top soil layer; z_1 [m] is depth of the first layer. All fluxes are defined positive downward.

We calculate separate surface temperatures for bare ground and vegetation. However, the soil temperature is identical for the two tiles. Heat flux exchanges between the surface and layer 1 are given by $G_{[v;b]}$, while between layer 1 and 2 the heat conductance is parameterized. We assume a zero flux boundary condition below the second layer. The numerical method to update soil temperature is discussed in Appendix C.

2.5 Water balance

As shown in Fig. 1, soil water is recharged by precipitation and can be lost by evapotranspiration and leakage. Consistent with the tiling and 2-soil layer structure, the water

GMDD
6, 4603–4663, 2013

balance equation can be written as,

$$\frac{dW_1}{dt} = z_1 \cdot C\, A_{ref} \frac{d\theta_1}{dt} = (P - Leak_1 - E_b \cdot (1 - f_c))C\, A_{ref} \quad (21)$$

$$\frac{dW_2}{dt} = z_2 \cdot C\, A_{ref} \frac{d\theta_2}{dt} = (Leak_1 - Leak_2 - E_v \cdot f_c)C\, A_{ref} \quad (22)$$

where $W_{[1;2]}$ [kg H_2O] is total water stored in layer 1 and 2; P [kg $H_2O\, m^{-2}\, s^{-1}$] is precipitation rate; $Leak_{[1;2]}$ [kg $H_2O\, m^{-2}\, s^{-1}$] is water leakage from surface to soil layer 1, and out of second soil layer to the deep ground, respectively; z_2 [m] is the depth of second soil layer.

Surface runoff is not considered explicitly. Instead, we assume that precipitation will infiltrate directly into the second soil layer when soil moisture in the top layer reaches field capacity. Other details are in Appendix D.

2.6 Soil moisture effects on W U E for the two soil water stress strategies

In our model, we include the impact of soil moisture on photosynthesis activity. Observations show that plants can adopt different strategies to cope with drought by controlling their stomata (Calvet, 2000; Calvet et al., 2004). During drought, a class of plants (e.g. soybean, maritime pine (Calvet, 2000; Calvet et al., 2004)) close their stomata to decrease transpiration, but increase mesophyll conductance (g_m [m s^{-1}]) to sustain photosynthesis. Another class of plants (e.g. hazel tree, sunflower, sessile oak (Calvet, 2000; Calvet et al., 2004)) leave their stomata open for transpiration and decrease the mesophyll conductance. After the soil moisture drops below a threshold, both types start to close stomata and stop carbon assimilation. These strategies affect biomass accumulation significantly and determine different W U E (Eq. 23). More details are described in Calvet (2000) and Calvet et al. (2004). Here we only discuss the relationship

GMDD
6, 4603–4663, 2013

between water use efficiency and extractable soil water content.

$$WUE = \frac{GPP}{E_v} \tag{23}$$

Following the parameterization of Calvet (2000) and Calvet et al. (2004), Fig. 2 presents the simulated intrinsic water use efficiency (ratio of net assimilation A_n to stomatal conductance g_s) for two strategies of grass and woody plants as function of extractable soil water.

In the defensive case, both woody plants and grass increase WUE when extractable water decreases. Stomata close and g_m increases (grass) or maintains (woody) its value. This regime extends until extractable water falls below an (observation based) threshold, from where g_m decreases sharply. The offensive case is more complex. Offensive plants insist on remaining their stomatal opening until very dry conditions are encountered. For woody vegetation, g_m then drops dramatically, which leads to a decrease in photosynthesis and consequently a decrease of WUE. However, g_m of grass remains relatively constant, which results in a smaller decrease of WUE.

In general, woody plants have a higher water use efficiency than grass. Although WUE of defensive woody vegetation is inversely proportional to soil water content when extractable soil water fractions excess 10 %, it is still larger than WUE of offensive woody vegetation until extractable water content exceeds 60 %, which is rarely met in arid and semi-arid regimes. Therefore, we assume that WUE of defensive woody vegetation strategy is always higher than offensive woody vegetation strategy.

2.7 Potential impacts of structural vegetation parameters on biomass amount

Using the vegetation structure as defined by the parameterization above, we illustrate the potential impacts of two structural parameters on total biomass. Biomass amount is updated by carbon gain and carbon loss processes. In this model, carbon loss is set equal to litter fall (Eq. 3). Since the involved time scales τ_{leaf}, τ_{stem} and τ_{root} (Eq. 11) are constants, vegetation structure does not affect carbon loss. The amount of carbon

GMDD
6, 4603–4663, 2013

gain (NPP) is limited by water and light, where light absorption is directly related to LAI. Concerning the water component, the carbon gain is not only influenced by the degree to which net photosynthesis is governed by available soil water, but also by the ability of vegetation to use water from the neighboring bare ground fraction, which can be represented by the relative water use (R_{WU}). R_{WU} is the ratio of vegetation transpiration over total evapotranspiration, defined as:

$$R_{WU} = \frac{E_v \cdot f_c}{E_v \cdot f_c + E_b \cdot (1 - f_c)} \tag{24}$$

From the definition (Eq. 24), we can find that R_{WU} is highly dependent on f_c. Notice that R_{WU} is not equal to rain use efficiency, because water also can be lost by infiltrating in deeper soil layer.

WUE depends on extractable soil water content (f_w) (Sect. 2.6). From the definition of f_w (Eq. 12), it is clear that f_w is effected by φ with given soil moisture.

Figure 3 presents the conceptual relation between structural parameters (α and D), vegetation internal factors (LAI, f_c, φ, GPP and WUE), R_{WU} and total biomass. From Fig. 3, we can find that α has a positive relationship with both LAI and f_c, as a higher α implies higher above ground biomass (Eq. 5). φ declines with an increasing α due to larger CA and lower values of C_{root} (Eq. 10). The canopy structure parameter D has a positive impact on LAI and conversely a negative impact on f_c, since a high value of D represents a lower crown and vegetation area. Therefore D is positively related to φ for a given value of α.

A high LAI increases the absorption of light per unit area, which results in a higher GPP. In our two-soil layer scheme (described in Sect. 2.5), bare soil evaporation is only extracted from the top layer. A higher f_c reduces water loss from bare soil ($E_b(1 - f_c)$ in Eq. (24) becomes smaller), which in turn implies that f_c has a positive effect on R_{WU}. A higher f_c also implies that the water taken from the bare ground has to be distributed over a larger vegetated area, which imposes a negative feedback. This can

GMDD
6, 4603–4663, 2013

be expressed by defining R_{space}, which describes this water distribution fraction.

$$R_{space} = \frac{1 - f_c}{f_c} \tag{25}$$

φ can have both a positive and a negative impact on WUE, depending on photosynthesis strategies and water content (Sect. 2.6). For offensive grass, a negative relation between φ and WUE is present. For other vegetation types, the relation is generally positive. Although WUE decreases when extractable water content exceeds a certain threshold, the magnitude of this reduction is relatively low (see Fig. 2).

2.8 Simulation process

Figure 4 illustrates the chain of computations followed in our model simulation process. The model state variables to be initialized are total biomass, soil moisture and soil temperature in two layers, and a number of vegetation structure factors before spin up. The initial total biomass is set to 30 kg C to avoid vegetation extinction at the start of the simulation. Initial soil moisture in both layers is equal to saturated soil moisture. Initial soil temperature of the two layers is equal to the initial air temperature. Model parameter α controls the distribution of total biomass over above ground ($C_{leaf} + C_{stem}$) and below ground (C_{root}) biomass (Eq.5). For woody vegetation the above ground biomass is distributed over C_{leaf} and C_{stem}. The geometrical distribution of leaf biomass is governed by a trade-off between high LAI concentrated on a relatively small crown area (CA) or low LAI combined with higher CA. The structure parameter D controls this trade-off (Eqs. 7 and 8). Once CA and LAI are known, the vegetation fraction (f_c) and root density (φ) can be specified (Eqs. 9 and 10). f_c is used to define two adjacent tiles (one vegetated, one bare ground) for which separate energy balances are computed.

The next step is the calculation of the photosynthesis process, that eventually leads to the specification of the stomatal conductance (g_s) and the biomass gain. Inputs for this photosynthesis calculation is the meteorological forcing, soil moisture conditions

GMDD
6, 4603–4663, 2013

and the vegetation structure parameters. From soil water content and relative root density we can calculate the mesophyll conductance (g_m) and internal CO_2 concentration (different approaches used for woody plants and grass, and for defensive or offensive soil moisture strategy) as specified in Appendix A. Photosynthesis rate depends on temperature (Appendix B1), internal CO_2 concentration and mesophyll conductance (B2) and radiation (B3). From the photosynthetic CO_2 flux (corrected for dark respiration) and the gradient of CO_2 between the ambient atmosphere and the internal concentration, the stomatal conductance can be calculated (Eqs. B10 and B11). This stomatal conductance is upscaled to the canopy scale by applying a vertical integration over the LAI profile (Appendix B4).

The aerodynamic exchange coefficient (g_a) is calculated using Monin-Obukhov similarity theory (Appendix C1). From the meteorological forcing and the aerodynamic and canopy conductance the energy balance in each tile can be found by solving for the surface temperature (Eq. 13–20).

The final step in the procedure is the update of the state variables. Vegetation carbon content is updated by the biomass gain from the photosynthesis, and a mortality governed by the litter fall parameterization (Eq. 11). The evapotranspiration rate found in the energy balance algorithm is used to adjust the water balance (Appendix D), while the soil heat flux modifies the soil temperature (Appendix C2).

2.9 Study area and datasets

The model has been set up for a grid configuration covering West Africa, where a large climate gradient exists (see Fig. 5). The model is set up at a 0.5° grid and forced using 3 hourly values of incoming long wave and shortwave radiation, precipitation, air temperature, wind speed and humidity for the period 2002 to 2007. The data are generated in the AMMA Land Model Intercomparison Project (Boone et al., 2009), and were used to run and compare a range of land surface models. In this data set, at 10° E, 15° N the maximum annual precipitation is approximately 200 mm yr^{-1}, while it increases to 4000 mm yr^{-1} near the coast. Shortwave incoming radiation shows an

GMDD
6, 4603–4663, 2013

opposite gradient, reducing from 270 W m^{-2} at 20° N to 170 W m^{-2} near the coast at 5° N.

The chosen value of the litter time scale (10 yr) leads to variations of biomass of woody plants at the decadal time scale. For particular vegetation structures and climate conditions, biomass changes are very slow. A 300 yr simulation is found to be adequate to approach equilibrium state for all types of vegetation structures. We spin-up the model by a repeated simulation of at least twenty times the available 6 yr forcing record (for some specific structures, 50 times is needed), and present results deduced from a mean annual cycle for the simulated 6 yr following the spin-up period. In this way, we calculate equilibrium biomass and other state variables and fluxes.

3 Results

3.1 Sensitivity of vegetation structure to α and D

To illustrate the sensitivity of vegetation structure to α and D, Fig. 6 shows values of LAI, f_c, C A and relative φ for a range of α and D values assuming a woody vegetation type with constant vegetation biomass C_{veg} = 30 kg C for the whole C A_{ref} of 15 m^2.

LAI increases with both α and D (Sect. 2.7). Once C A is equal to C A_{ref}, LAI has a positive linear relation with α (see bottom left corner of Fig. 6a).

Crown area (C A) and LAI are negatively related for a given amount of leaf biomass (Fig. 6a and b show opposite slopes with certain α). Both LAI and C A are more sensitive to D when $\alpha > 0.1$. Maximum C A appears with high α and low D. When D is extremely low, C A_{ref} can be reached by allocating a little amount of leaf biomass. When $\alpha > 0.2$, C A is dominated by D due to higher leaf biomass.

Leaf coverage f_c (Fig. 6c) is dominated by C A. However, it is also effected by LAI (Eq. 9), especially when LAI is low. Maximum f_c appears with high α and low D. Patterns of C A and f_c are similar, but f_c is more sensitive to α, which has positive relations with both C A and LAI (Fig. 3).

GMDD
6, 4603–4663, 2013

Rooting density φ affects water uptake ability of vegetation (Appendix B). If C_{veg} is given, φ depends on α and C A (Eq. 10). In Fig. 6d, a maximum root density is found with small α and high D, leading to a large rooting biomass and small crown area.

3.2 Optimal vegetation structure

In this section we simulate how vegetation structure and soil water stress influence biomass, LAI, f_c, water use efficiency and relative water use (R_{WU}). Ten α and ten D are chosen to compose an ensemble of 100 vegetation structures. With these ensembles, two soil water stress strategies are applied on four precipitation regimes (200, 400, 800 and 1200 mm yr^{-1}, all ranging within ±25 mm yr^{-1}) in West Africa. In each regime approximately five grid points were randomly collected. Here we show simulations for offensive and defensive grass for the 200 mm yr^{-1} climate regime, and woody plant structures for all four climate regimes. The intrinsic W U E of defensive strategy for woody plants is always higher than that of offensive strategy under same situation (Calvet et al., 2004), which implies that the defensive strategy leads to more biomass than the offensive strategy with each specific structure. For this reason only the defensive strategy is illustrated for woody plants.

3.2.1 Grass biomass dynamics for 200 mm yr^{-1}

Figure 7a shows the sensitivity of the equilibrium biomass amount for grass as function of α and D in the 200 mm yr^{-1} precipitation regime for the defensive strategy. Figure 7b shows relations of C_{veg}-LAI, C_{veg}-f_c, C_{veg}-W U E and f_c-R_{WU}. Related Spearman correlation coefficiences are displayed in each subfigure. Maximum biomass is simulated for maximum D, which implies a high LAI (3.9 m^2 m^{-2}) and a very low f_c of 0.11, indicating patches of dense grass vegetation. For defensive grass vegetation, the water use efficiency increases with extractable water. However, for low values of α(< 0.15), LAI is too low to gain enough carbon to sustain a high root density. When $\alpha > 0.35$, φ is too low to take up sufficient amounts of water. Thus a trade-off exists between root

GMDD
6, 4603–4663, 2013

density and LAI, and the maximum biomass is found for intermediate shoot-root ratio ($\alpha = 0.25$), where $\varphi = 0.6\,\mathrm{kg\,C\,m^{-2}}$ and $\mathrm{LAI} = 3.85$. This also can be seen in Fig. 3. α has positive and negative impacts on GPP and WUE respectively, which implies that a trade-off exist. While D has a positive effect on both GPP and WUE, implying that the maximum D is optimal. The simulated biomass is more strongly correlated with WUE and LAI than with f_c (Fig. 7b). We conclude that for dry conditions WUE is more important to biomass than f_c. For patches of grass, it is interesting to note that the relative water use (R_{WU}) of the patches is always higher than f_c. This implies that water is extracted from the surrounding bare soil to supply the transpiration from the vegetated fraction of the area.

The biomass patterns of offensive grass (Fig. 7c and d) are clearly different with defensive grass. In the offensive case, WUE decreases with increasing extractable water (Fig. 2). Since φ has negative impact on WUE, the maximum biomass is found with the highest α, which positively effects both WUE and GPP (Fig. 3). Whereas D, in turn, has negative relation to WUE but positive relation to GPP. Therefore a medium value of D is found with maximum biomass. Simultaneously, decreasing D increases vegetation cover (based on definition of D in Eq. 8) and thereby reduces the extraction of water from the surrounding soil to the vegetation. If this "source area" for water supply is too small, vegetation cannot survive under this climate. From Fig. 7d, we can find that WUE is the dominant factor explaining maximum biomass variability. However, some structures also can generate a high WUE with low total biomass. These structures can be found when $\alpha = 0.45$ and $D \approx 2$, where WUE is high but the total amount of water uptake is relative low. Comparing the two strategies, the maximum biomass of offensive grass is higher than that of defensive grass, since the WUE is slightly higher for offensive strategy (Fig. 2). In addition, $R_{WU} > f_c$ also applies to the offensive case, meaning that an important condition for vegetation survival under arid conditions is that vegetation is able to use water from the surrounding bare soil.

GMDD
6, 4603–4663, 2013

3.2.2 Wood biomass dynamics under different precipitation regimes

Figures 8 and 9 show total biomass for woody plants with a defensive drought stress strategy for different climate regimes.

For the 200 mm yr^{-1} precipitation regime, it is clearly illustrated that woody biomass has a smaller survival variable space than grass. Biomass below 0.4 kg C m^{-2} cannot survive due to a minimum GPP needed for maintenance respiration. The highest biomass is found when $\alpha = 0.45$ and $D = 5$. In contrast to defensive grass, the optimal defensive woody structure has a higher biomass due to longer litter time scales and thus slower biomass loss rates.

High correlation coefficients of C_{veg}-WUE and C_{veg}-LAI (Figure 8b) indicate that WUE and LAI are the primary control variables to optimize biomass. Although the correlation of C_{veg}-f_c is high ($r^2 = 0.9$), f_c is just passively maximized with increase of C_{veg}, which is not the dominant factor (also see in discussion of positive and negative feedbacks below). As before, it is of interest that the R_{WU} always exceeds the vegetation cover. Also woody vegetation adjusts its environment by using the water from the surrounding bare soil. For both grass and woody vegetation types, a vertical structure is more beneficial to survive under the dry 200 mm yr^{-1} regime. Although WUE is the dominant factor explaining total biomass variability, only optimizing WUE is not able to produce high biomass. Water uptake ability and potential photosynthesis rate are also important.

Figure 8c shows the biomass dependence on vegetation structure for the 400 mm yr^{-1} precipitation regime. In this wetter regime still many combinations of D and α lead to a vegetation structure that cannot survive. Only a vertical biomass orientation of patches of woody vegetation to a maximum cover f_c of 0.1 can exist. Figure 8c illustrates that maximum biomass is found at maximum D and α. In the wetter regime, the optimal α is higher and D is lower than that in the 200 mm yr^{-1} regime. Also here $R_{WU} > f_c$.

GMDD
6, 4603–4663, 2013

Figure 9a shows the results for the 800 mm yr^{-1} precipitation regime. In this wetter regime, some horizontal structures start to survive. With low D ($0.1 < D < 0.3$), CA almost reaches CA_{ref}, where f_c is strongly regulated by LAI (Eq. 9). Here α affects the total biomass drastically. When $\alpha < 0.35$, above ground biomass is too low to gain enough carbon for maintaining root biomass. While if $\alpha > 0.45$, implying lower φ, water uptake ability is not able to meet the demand for transpiration. The optimal structure is found for $\alpha = 0.5$ and $D = 1$. In comparison to the drier regimes shown in Fig. 8, the optimal D decreases. In addition, C_{veg} and f_c are highly correlated ($r^2 = 0.9$). While at low biomass, R_{WU} is higher than f_c. But f_c is nearly equal to R_{WU} at higher biomass. We conclude that vertical vegetation uses more water from the bare soil and have higher WUE, but biomass growth is limited by stem biomass. With a horizontal structure, the bare soil fraction is low due to a high f_c. Per unit surface area vegetation shares less water from the bare soil area, but this leads to a higher biomass value with high R_{WU}. Vertical structure is beneficial to survive especially in water limited areas, while it is not able to produce the maximum biomass in wetter regimes. In addition, total biomass is less sensitive to WUE. Instead, leaf coverage becomes the primary factor to optimized biomass.

In the wettest regime (Fig. 9c) most combinations of α and D can survive. With low α above ground biomass cannot survive, as too much carbon is used to maintain the rooting system. Vegetation with a horizontal structure can survive, and lead to higher biomass. f_c and R_{WU} are almost identical, meaning that water competition between bare and vegetated soil is less important. In this regime, water availability is no constraint and vegetation can survive without using water from the surrounding bare soil. Instead, high leaf coverage can avoid water loss from bare soil evaporation and increase transpiration. Biomass shows a high correlation with f_c, implying the importance of f_c to optimize total biomass.

GMDD
6, 4603–4663, 2013

3.3 Dominant factors for different climate regimes

From Sects. 3.1 and 3.2, we found that LAI, f_c and WUE influence biomass significantly but their importance is climate dependent. To depict the variability of the response mechanisms as a function of the climate regime, we calculated Spearman's correlation coefficients across 87 available grid cells in a given climate regime between averaged biomass and the variables LAI, f_c and WUE for each vegetation strategy. Cases where biomass did not survive are not taken into account. Figure 10 presents the variability of the correlation coefficients as a function of mean annual precipitation for 4 vegetation cases.

From Fig. 10, we can conclude that WUE and LAI are dominant factors in the low precipitation regimes between 200 and 600 mm yr^{-1}, as they generate the highest correlation to biomass. LAI generally behaves similar as WUE. This implies that vegetation requires both a high WUE and a high potential carbon assimilation rate to survive under arid and semi-arid regimes. For low precipitation, vegetation maximizes its biomass by adopting a vertical structure, limiting f_c. With an increase of precipitation, LAI and WUE is less correlated to biomass, while the correlation of C_{veg} and f_c increases (Fig. 10).

4 Discussion

This study presents findings to two questions. One is how vegetation adjusts to climate by engineering carbon allocation. The second is how the optimal vegetation structure shifts with climate. For the first question, the sensitivity of biomass to vegetation structure is analyzed under certain climate (Sect. 3.2). The shoot-root ratio and canopy structure effect biomass significantly. In arid and semi-arid areas, vegetation can benefit from growing in patches (high LAI/f_c) due to the water competition between bare soil and plants. In the meantime, vegetation should carefully allocate biomass to root and leaves in order to keep a balance between water uptake ability (related to φ) and

GMDD
6, 4603–4663, 2013

light absorption (related to LAI). While under wetter climate, where water is sufficient, horizontal canopy structure is preferable, which can avoid water use from evaporation. In addition, strategies of vegetation to drought has significant impact on vegetation structure.

To answer the second question, we present Spearman correlation coefficients of C_{veg}-f_c, C_{veg}-LAI and C_{veg}-WUE as a function of mean annual precipitation (Sect. 3.3). LAI and WUE have high correlation to C_{veg} when rainfall is less than 600 mm yr^{-1}, which implies the importance of WUE and LAI to total biomass. While f_c has higher correlation with C_{veg} when rainfall excesses 600 mm yr^{-1}. Simultaneously, two feedbacks are found to interpret the correlation change with precipitation.

4.1 Optimization approach

The objective function of vegetation optimization process follows earlier work by Schymanski et al. (2010). Compared to work of Schymanski et al. (2010), we analyze effect of spatial structure of vegetation on water, carbon and energy balances. In addition, our model is run by real climate forcing data. In the work of Schymanski et al. (2010), a precipitation threshold at 240 mm yr^{-1} was found for homogeneous vegetation existence. While in our study, the threshold of homogeneous (equivalent to $CA = CA_{ref}$) grass is found at 450 mm yr^{-1} (not shown), which coincides to the peak of grass fraction observed in Africa (Guan et al., 2012). In addtion, the canopy closure of woody plants appears when precipitation is larger than 630 mm yr^{-1}, which is slightly lower than observations by Sankaran et al. (2005).

4.2 Two feedbacks

Two feedbacks between f_c and water used by vegetation coexist. A negative feedback concerns the infiltrated water of the bare soil part (we call it f_c-R_{space} feedback), while a positive feedback addresses water loss by soil evaporation (we call it f_c-R_{WU} feedback).

GMDD
6, 4603–4663, 2013

In arid and semi-arid areas, precipitation during the short monsoon season infiltrates fast into deep soil layers, which limits bare soil evaporation. Water stored in deeper layers originating from bare ground fractions of the grid box can be used for evapotranspiration by vegetation patches, leading to higher annual mean $/E_v$ than $/E_b$. This mechanism implies that the equilibrium biomass of vegetation patches depends on water available from both the vegetated and the bare ground fractions. A negative perturbation of the biomass decreases leads to a decrease of f_c and an increase of the bare soil area. This leads to more water per unit plant area, which will lead to a recovery of biomass. For positive perturbations of equilibrium biomass and f_c, the water that vegetation can extract from the surrounding bare soil decreases. The amount of water per unit plant area is limited, by which the vegetation cannot maintain its current biomass, which will result in a decrease of biomass and f_c. This f_c-R_{space} feedback makes the vegetation fraction very resilient to climate (Holmgren and Scheffer, 2001), and thus biomass becomes more sensitive to LAI and WUE. We call this regime a "survival" state. This feedback leads to a very stable vegetation structure, which is found from many observations (Holmgren and Scheffer, 2001).

A f_c-R_{WU} feedback loop results from the notion that vegetation avoids water loss from evaporation by increasing f_c. Increasing f_c leads to enhanced water availability, which accelerates f_c growth until canopy closure. Using a two-soil layer model, Baudena and Provenzale (2008) found similar vegetation feedback mechanisms due to shading, which also has a beneficial effect on vegetation. This positive feedback is more noticeable under constant rainfall than under intermittent rainfall, which implies that the temporal distribution of precipitation strongly influences the impact of shading feedback to biomass. For dry climates, the relative precipitation variation is larger than that under wetter climate conditions. The importance of shading feedback to biomass rises with increase of precipitation.

Under wetter climate conditions, with longer monsoon seasons, annual mean soil evaporation will be larger. When annual mean $/E_b$ exceeds $/E_v$, vegetation can use more water by increasing f_c to avoid water loss from bare soil evaporation. When

GMDD
6, 4603–4663, 2013

biomass and f_c increase, water will not be lost by soil evaporation from the newly vegetated area. Simultaneously, as the amount of water saved exceeds the amount needed to maintain the biomass (because $/E_b > /E_v$). Biomass growth will be further enhanced leading to a f_c-R_{WU} feedback loop until the canopy nearly closes. For woody vegetation, this f_c-R_{WU} feedback cannot lead to fully coverage. From Eq. (9), we see that f_c can be increased by increasing crown area or by increasing LAI. The cost of increasing f_c is less than the increase of LAI, as no extra C_{stem} is needed. This regime we call the "growing" state.

Both feedbacks exist across the gradient of precipitation in West Africa. However, the f_c-R_{space} feedback is dominant in arid and semi-arid areas. It implies that water loss from evaporation is negligible due to short duration of monsoon season and the fast infiltration rate. In Baudena and Provenzale (2008), under intermittent rainfall (represents the rainfall in arid and semi-arid areas), the infiltration feedback (equivalent to the f_c-R_{space} feedback in our model) sharply decreases the threshold of precipitation to vegetation survival. It also implies the importance of the f_c-R_{space} feedback to vegetation in dry climate.

The f_c-R_{WU} feedback dominates when soil evaporation is too high to be ignored. The critical threshold of the dominant feedback shifts at the point where water gain by increasing f_c is equal to the cost of biomass to support f_c increase. This threshold can be simply evaluated by comparing $/E_v$ and $/E_b$. When $/E_v > /E_b$, water loss from evaporation is worth saving. Otherwise vegetation gets more benefit by keeping in patches. Notice that the threshold is not fixed, it depends on PFT and soil types (due to infiltration rate). The threshold between "survival" and "growing" state is determined by whether an increase in f_c is beneficial to vegetation growth (equal to whether $/E_v > /E_b$ or not).

In addition, the shift of dominant factors (shown in Sect. 3.3) also indicates the shift of dominant feedback. The threshold of dominant factor shifting is found around 600 mm yr^{-1}, where is also the threshold that canopy closure appears.

GMDD
6, 4603–4663, 2013

5 Conclusions

This work shows how vegetation structure effects total biomass with different climate. The newly developed water-carbon-energy balance model focuses on effects of vegetation structure on photosynthesis and transpiration ability via detailed physical mechanism and runs by using realistic climate forcing data. Instead of an empirical multiplicative Jarvis model for surface conductance, we use CHTESSEL model to calculate the surface conductance explicitly from a vegetation photosynthesis module, including its response to temperature, radiation, CO_2 and water stress. By using CHTESSEL, coupling our model to an operational version of for instance the ECMWF atmospheric model is made straightforward. This coupled model will be used in the future to investigate the role of vegetation in land-atmosphere interactions. In addition, we also introduce two vegetation structure parameters in order to explore the effect of spatial structure on vegetation biomass for different climate regimes.

We found that the optimal vegetation structure shifts with climate. Vertical canopy with medium shoot-root ratio is easy to survive in arid climate, but cannot produce high biomass and coverage in wetter climate. Horizontal canopy with high shoot-root ratio is hard to survive in arid climate, while it can produce high biomass and coverage in wetter climate. Two feedbacks are also found in this study. The f_c-R_{space} feedback dominates in arid and semi-arid climate, which makes vertical canopy is optimal. When the f_c-R_{space} feedback dominates, f_c is very stable and biomass is mainly influenced by LAI and f_c. The f_c-R_{WU} feedback dominates in wetter climate where the horizontal canopy is the optimal structure. When the f_c-R_{WU} feedback dominates, biomass is more sensitive to f_c than LAI and W U E. In addition, different photosynthesis strategies to drought also can influence the optimal structure. The threshold where the dominant feedback shifts depends on climate, but it is significantly influenced by PFTs and soil types, which may cause bi-stability under similar climate.

GMDD
6, 4603–4663, 2013

Appendix A

Vegetation response to soil water content

In this section, we introduce two strategies that vegetation adapts to water stress. This work is explicitly described in Calvet (2000) and Calvet et al. (2004). From observations, Calvet (2000) and Calvet et al. (2004) found that soil water stress strongly influences mesophyll conductance (g_m), maximum water vaper deficit (D_{max}) and stomatal opening (represented by f_0). The mechanism is PFT dependent.

A1 Defensive strategy for grass

In grass case, extractable soil water content influences g_m and D_{max} significantly. g_m determines potential photosynthesis rate, while D_{max} has affect on stomatal opening, which determines transpiration rate (Sect. B). There is a negative relation between g_m and D_{max} following the experimental Eq. (A1) when f_w is larger than f_{wc}. f_{wc} is the threshold of drought depending on vegetation type and strategies (Table 1). During drought ($f_w > f_{wc}$), D_{max} decreases fast, while g_m increases. When f_w falls below f_{wc}, D_{max} becomes constant (stomata almost totally closed) and g_m starts to drop until photosynthesis stops. In Appendix A, g_m and D_{max} are calculated under 25 °C.

$$\ln(g_m) = a_1 - b_1 \ln(D_{max}) \quad \text{(A1)}$$

Where $a_1 = 2.381$, $b_1 = 0.6103$. g_m that is effected by f_{wc} can be calculated as:

$$g_m = g_m^X + \left(g_m^* - g_m^X\right)\frac{f_w - f_{wc}}{1 - f_{wc}}, f_w \geq f_{wc}$$

$$g_m^X \frac{f_w}{f_{wc}}, f_w < f_{wc} \quad \text{(A2)}$$

Where g_m^X [mm s^{-1}] is corresponding to D_{max}^N following Eq. (A1); g_m^N [mm s^{-1}] is corresponding to D_{max}^X following Eq. (A1); g_m^* [mm s^{-1}] is unstressed mesophyll conduc-

GMDD
6, 4603–4663, 2013

tance. D^X_{max} [g kg^{-1}] and D^N_{max} [g kg^{-1}] are maximum and minimum value of D_{max} respectively (Table 1).

If $f_w \geq f_{wc}$, D_{max} is retrieved from Eq. (A1) by g_m; if $f_w < f_{wc}$, D_{max} is equal to D^N_{max} as a constant.

A2 Offensive strategy for grass

In the offensive strategy of grass, the relation between g_m and D_{max} still follows Eq. (A1). However, with f_w decreasing ($f_w > f_{wc}$) it goes to the opposite direction, which rises D_{max} to open stomata and reduce photosynthesis rate by decreasing g_m. After $f_w < f_{wc}$, offensive grass start to close stomata (D_{max} decreases) and keep a low g_m, implying an increase in W U E. D_{max} for offensive grass can be calculated by,

$$D_{max} = D^X_{max} + \left(D^*_{max} - D^X_{max}\right)\frac{f_w - f_{wc}}{1 - f_{wc}}, f_w \geq f_{wc}$$
$$D^X_{max}\frac{f_w}{f_{wc}}, f_w < f_{wc} \quad \text{(A3)}$$

D^*_{max} is calculated with unstressed g^*_m by Eq. (A1).

After getting D_{max}, g_m can be calculated based on Eq. (A1) when $f_w \geq f_{wc}$; g_m keeps as g^N_m when $f_w < f_{wc}$.

A3 Defensive strategy for woody plants

In the woody plant case, instead of D_{max}, g_m is highly correlated to f_0, which directly determines the opening of stomata (see Appendix B and Eq. B5). In the unstressed condition, the relation can be described by Eq. (A4). While under water stressed condition, Eq. (A5) is applied.

$$\ln\left(g^*_m\right) = 4.7 - 7.0 f^*_0 \quad \text{(A4)}$$

GMDD
6, 4603–4663, 2013


$$\ln(g_m) = 2.8 - 7.0 f_0 \quad \text{(A5)}$$

In the defensive strategy, g_m is equal to g_m^* when $f_w \geq f_{wc}$. It is calculated based on Eq. (A4) by f_0^* from Table 1. When $f_w < f_{wc}$,

$$g_m = g_m^* \frac{f_w}{f_{wc}} \quad \text{(A6)}$$

f_0 can be calculated as,

$$f_0 = \begin{cases} f_0^N + \left(f_0^* - f_0^N\right) \dfrac{f_w - f_{wc}}{1 - f_{wc}}, f_w \geq f_{wc} \\ \min\left(1.0, f_0\left(g_m\right)\right), f_w < f_{wc} \end{cases} \quad \text{(A7)}$$

Where f_0^N [-] corresponds to g_m^* by Eq. (A5); $f_0(g_m)$ [-] is the f_0 value based on Eq. (A5) with corresponding g_m.

A4 Offensive strategy for woody plants

For woody plants with offensive strategy, g_m^X [mm s^{-1}] is calculated from Eq. (A5) by using f_0^*. Then the stressed g_m is given by,

$$g_m = \begin{cases} g_m^N + \left(g_m^* - g_m^N\right) \dfrac{f_w - f_{wc}}{1 - f_{wc}}, f_w \geq f_{wc} \\ g_m^N \dfrac{f_w}{f_{wc}}, f_w < f_{wc} \end{cases} \quad \text{(A8)}$$

Finally stressed f_0 can be calculated as:

$$f_0 = \begin{cases} f_0^*, f_w \geq f_{wc} \\ \min\left(1.0, f_0\left(g_m\right)\right), f_w < f_{wc} \end{cases} \quad \text{(A9)}$$

GMDD
6, 4603–4663, 2013

Appendix B

A-g_s model

The carbon assimilation rate is inflenced by incoming solar radiation, surface temperature, vapor pressure deficit, etc. In addition, plant activities play an important role in this process. The A-g_s model developed by Jacobs et al. (1996) simulates the performance of vegetation in the total process. It includes impacts from radiation, temperature, vapor pressure deficit, CO_2 concentration and stomatal opening.

B1 Temperature effect

The maximum of the carbon assimilation rate (A_{max}) of plants shifts with a change in surface temperature. The surface temperature T_s discussed in this Appendix is the surface temperature of vegetation part. Equation (B1) shows how A_{max} is calculated by a given reference value at 25 °C (see Table 1). The maximum effect of mesophyll conductance change with T_s is similar as A_{max} (Eq. B2). Compensation concentration ($\Gamma(T_s)$) can be calculated by Eq. (B3).

$$A_{max}(T_s) = \frac{A_{max}(25\,^{\circ}\mathrm{C}) \cdot Q_{A_m}^{(T_s-25)/10}}{\left(1+e^{0.3(T_{1,A_m}-T_s)}\right)\left(1+e^{0.3(T_s-T_{2,A_m})}\right)} \quad \text{(B1)}$$

$$g_m(T_s) = \frac{g_m(25\,^{\circ}\mathrm{C}) \cdot Q_g^{(T_s-25)/10}}{\left(1+e^{0.3(T_{1,g}-T_s)}\right)\left(1+e^{0.3(T_s-T_{2,g})}\right)} \quad \text{(B2)}$$

$$\Gamma(T_s) = \Gamma(25\,^{\circ}\mathrm{C})\, Q_{\Gamma}^{(T_s-25)/10} \quad \text{(B3)}$$

GMDD
6, 4603–4663, 2013

Where $A_{max}(T_s)$ [kg C m^{-2} s^{-1}] is the maximum carbon assimilation rate; $g_m(T_s)$ [m s^{-1}] is the mesophyll conductance; $\Gamma(T_s)$ [ppm] is the compensation concentration; Q_{A_m}, Q_g and Q_Γ are Q_{10} values for A_{max}, g_m and Q_Γ respectively, here all of them are equal to 2, T_{1,A_m} and T_{2,A_m} [°C] are reference temperature for A_{max} calculation; $T_{1,g}$ and $T_{2,g}$ are reference temperature for g_m calculation.

B2 CO_2 effect

The gradient of internal and external CO_2 concentration determines carbon assimilation rate. Equation (B4) shows the relation between carbon limited assimilation rate A_m and A_{max}.

$$A_m = A_{max}\left(1 - e^{-\frac{g_m(c_i-\Gamma)}{A_{max}}}\right) \quad \text{(B4)}$$

Where c_i [ppm] is CO_2 internal concentration, which is controlled by stomatal opening. With the change of water vapor deficit vpD [Pa], c_i shifts between external CO_2 concentration c_a [ppm] and Γ (Eq. B5).

$$c_i = f \cdot c_a + (1-f)\Gamma \quad \text{(B5)}$$

Where f [-] is the factor that determines the opening of stomata, which is influenced by vpD as:

$$f = f_0\left(1 - \frac{\text{vpD}}{D_{max}}\right) \quad \text{(B6)}$$

Where f_0 [-] is based on plant types and extractable water content (see Appendix A).

B3 Radiation effect

A_m is the CO_2 limited assimilation rate under maximum incoming solar radiation. The final carbon assimilation will also depends on photo active radiation (I_a), as shown in

GMDD
6, 4603–4663, 2013

Eq. (B7).

$$A_n = (A_m + R_d)\left(1 - e^{-\frac{\epsilon^* I_a}{A_m + R_d}}\right) - R_d \quad \text{(B7)}$$

Where ϵ^* [kg J^{-1}] is the quantum efficiency according to,

$$\epsilon^* = \epsilon_0^* \frac{c_i - \Gamma}{c_i + 2\Gamma} \quad \text{(B8)}$$

Where ϵ_0^* [kg J^{-1}] is the maximum quantum use efficiency. R_d is dark respiration, assumed as a ratio of A_m (Eq. B9).

$$R_d = \frac{A_m}{9} \quad \text{(B9)}$$

After A_n is known, we calculate stomata conductance g_{sc} by Eq. (B10).

$$g_{sc} = \frac{A_n + R_d\left(1 - \frac{A_n + R_d}{A_m + R_d}\right)}{c_a - c_i} \quad \text{(B10)}$$

Then the stomatal conductance to water vapor g_s is,

$$g_s = 1.6 g_{sc} \quad \text{(B11)}$$

B4 Vertical integration

The I_a is vertically integrated within the canopy. The A_n and g_s will be calculated by integration method to get the total assimilation rate and canopy water vapor conductance (Eqs. B12 and B13).

$$A_n = \mathrm{L\,A\,I} \int_0^1 A_n\left(\hat{h}\right) \mathrm{d}\hat{h} \quad \text{(B12)}$$

GMDD
6, 4603–4663, 2013

$$g_s = \mathrm{LAI} \int_o^1 g_s\left(\hat{h}\right) \mathrm{d}\hat{h} \tag{B13}$$

Where $\hat{h}$[-] is the relative height of the plant.

The I_a on the top of relative height $\hat{h}$ is given as:

$$I_a\left(\hat{h}\right) = \mathrm{PAR}\left(1 - K\left(\hat{h}\right)\right) \tag{B14}$$

Where PAR [W m^{-2}] is photo active radiation on the top of canopy. It is equal to 48 % of R_{swd} (Dekker et al., 2000; Boussetta et al., 2013). K[-] is the extinction function given as:

$$K\left(\hat{h}\right) = \delta\left(\mu_s\right) K_{df}\left(\hat{h}\right) + \left(1 - \delta\left(\mu_s\right)\right) K_{dr}\left(\hat{h}\right) \tag{B15}$$

Where μ_s [°] is solar zenith angle, here we assume $\mu_s = 90^\circ$; $\delta = 0.2$ [-] is the ratio of diffuse to total downward shortwave radiation at the top of the layer. K_{dr} and K_{df} are extinction coefficients of direct and diffuse light (Eqs. B16 and B17).

$$K_{dr}(\hat{h}) = 1 - e^{-\frac{G_l}{\cos\mu_s} b_l \ \mathrm{LAI} \ (1-\hat{h})} \tag{B16}$$

$$K_{df}(\hat{h}) = 1 - e^{-0.8b \ \mathrm{LAI} \ (1-\hat{h})} \tag{B17}$$

Where $G_l = 0.5$ is the leaf distribution parameter; b_l is the foliage scattering coefficient given as,

$$b = 1 - \frac{1 - \sqrt{1-\varpi}}{1 + \sqrt{1-\varpi}} \tag{B18}$$

GMDD
6, 4603–4663, 2013

Where ω is the scattering albedo equal to 0.2.

Finally, we calculate G P P and N P P from A_n and R_d as,

$$GPP = A_n + R_d \tag{B19}$$

$$NPP = A_n \tag{B20}$$

Appendix C

Surface energy balance

C1 Monin-Obukhov Similarity theory

The diurnal surface temperature changes very fast in arid area, which leads to strong convection at the surface layer. A simple methods that use surface wind speed and roughness length to calculate Monin-Obukhov Similarity theory is used to describe fluxes turbulence at the surface layer (ECMWF, 2008). The surface fluxes of momentum, heat and moisture are defined as:

$$J_M = \rho u_*^2 \tag{C1}$$

$$J_s = \rho u_* s_* \tag{C2}$$

$$J_q = \rho u_* q_* \tag{C3}$$

GMDD
6, 4603–4663, 2013

Where J_M, J_s, J_q are momentum flux, sensible heat flux (equal to H) and latent heat flux (equal to lE) respectively; u_* is friction velocity; s_* is heat turbulence; q_* is humidity turbulence.

The stability parameter L is the Obukhov length, defined as,

$$L = -\frac{u_*^3}{\frac{\kappa g}{T_a} Q_{0v}} \tag{C4}$$

Where κ is Von Karman constant; T_a is air temperature at 2 m high; g is acceleration due to gravity; Q_{0v} is virtual temperature flux in the surface layer (Eq. C5).

$$Q_{0v} = \frac{-u_* s_* - (c_{p_{vap}} - c_{p_{dry}}) T_a u_* q_*}{c_p} + \hat{\epsilon} T_a u_* q_* \tag{C5}$$

Where $\hat{\epsilon} = 0.6$ is a constant related with water vapor and gas constant; $c_{p_{vap}}$ and $c_{p_{dry}}$ are specific heats at constant pressure of water vapor and dry air respectively. c_p is specific heat capacity of moist air, given by:

$$c_p = c_{p_{dry}} + \left(c_{p_{vap}} - c_{p_{dry}}\right) \cdot \mathrm{SH} \tag{C6}$$

The 3 surface fluxes are calculated by,

$$J_M = \rho C_M |U_n|^2 \tag{C7}$$

$$J_s = \rho C_H |U_n| c_p (T_a - T_s) \tag{C8}$$

$$J_q = \rho C_Q |U_n| (q_a(T_a) - q_{sat}(T_s)) \tag{C9}$$

GMDD
6, 4603–4663, 2013

Where $|U_n|$ is wind speed; C_M, C_H and C_Q are transfer coefficients to momentum, heat and humidity respectively (Eqs. C10, C11 and C12). Compared with Eqs. (16) and (19), we can find that $C_H|U_n| = g_a$ and $C_Q|U_n| = \frac{1}{1/g_s+1/g_a}$.

$$C_M = \frac{\kappa^2}{\left[\log\left(\frac{z_n+z_{0M}}{z_{0M}}\right) - \Psi_M\left(\frac{z_n+z_{0M}}{L}\right) + \Psi_M\left(\frac{z_{0M}}{L}\right)\right]^2} \tag{C10}$$

$$C_H = \frac{\kappa^2}{\left[\log\left(\frac{z_n+z_{0M}}{z_{0M}}\right) - \Psi_M\left(\frac{z_n+z_{0M}}{L}\right) + \Psi_M\left(\frac{z_{0M}}{L}\right)\right]\left[\log\left(\frac{z_n+z_{0M}}{z_{0H}}\right) - \Psi_H\left(\frac{z_n+z_{0M}}{L}\right) + \Psi_H\left(\frac{z_{0H}}{L}\right)\right]} \tag{C11}$$

$$C_Q = \frac{\kappa^2}{\left[\log\left(\frac{z_n+z_{0M}}{z_{0M}}\right) - \Psi_M\left(\frac{z_n+z_{0M}}{L}\right) + \Psi_M\left(\frac{z_{0M}}{L}\right)\right]\left[\log\left(\frac{z_n+z_{0M}}{z_{0Q}}\right) - \Psi_Q\left(\frac{z_n+z_{0M}}{L}\right) + \Psi_Q\left(\frac{z_{0Q}}{L}\right)\right]} \tag{C12}$$

Where $z_n = 2\,\mathrm{m}$ is the height of the measurement; z_{0M}, z_{0H} and z_{0Q} are momentum, heat and humidity roughness length respectively.

The wind speed $|U_n|$ is expressed as:

$$|U_n|^2 = u_n^2 + v_n^2 + w_*^2 \tag{C13}$$

Where u_n, v_n are surface wind speeds; w_* is the free convection velocity scale calculated as:

$$w_* = \left(z_n \frac{g}{T_a} Q_{0v}\right)^{1/3} \tag{C14}$$

The stability functions are derived from empirical expressions. And $\zeta = \frac{z}{L}$ is used to describe the stability of the surface layer.

GMDD
6, 4603–4663, 2013

In unstable conditions ($\zeta < 0$), gradient functions are shown below:

$$\Psi_M(\zeta) = \frac{\pi}{2} - 2\mathrm{atan}(x) + \log\frac{(1+x)^2(1+x^2)}{8} \tag{C15}$$

$$\Psi_H(\zeta) = \Psi_Q(\zeta) = 2\log\left(\frac{1+x^2}{2}\right) \tag{C16}$$

with $x = (1 - 16\zeta)^{1/4}$

In stable condition ($\zeta > 0$), functions are defined as below:

$$\Psi_M(\zeta) = -b\left(\zeta - \frac{c}{d}\right)e^{-d\zeta} - a\zeta - \frac{bc}{d} \tag{C17}$$

$$\Psi_H(\zeta) = \Psi_Q(\zeta) = -b\left(\zeta - \frac{c}{d}\right)e^{-d\zeta} - \left(1 + \frac{2}{3}a\zeta\right)^{1.5} - \frac{bc}{d} \tag{C18}$$

with $a = 1$; $b = 2/3$; $c = 5$ and $d = 0.35$.

C2 Soil temperature update

Soil heat flux is calculated by temperature gradient from the middle of layer 1 to the surface (Eq. 20). In this 2-layer theme, we also need to update temperature change in both of the layers. Equation (C19) shows the diffusion of soil heat transport. Assuming that the soil heat flux from layer 2 to deeper layer is 0, we can solve Eq. (C19) by numerical methods. In Eqs. (C20) and (C21), i indicates time step i, leads to two unknowns (T_1^{i+1} and T_2^{i+2}) in two equations.

$$\frac{\partial T}{\partial t} = \hat{\kappa}\frac{\partial^2 T}{\partial z^2} \tag{C19}$$

GMDD
6, 4603–4663, 2013

$$\frac{T_1^{i+1} - T_1^i}{\Delta t} = \hat{\kappa} \frac{\frac{2(T_2^i - T_1^i)}{z_1 + z_2} - \frac{2(T_1^i - T_s^i)}{z_1}}{z_1} \quad \text{(C20)}$$

$$\frac{T_2^{i+1} - T_2^i}{\Delta t} = \hat{\kappa} \frac{0 - \frac{2(T_2^i - T_1^i)}{z_1 + z_2}}{z_1} \quad \text{(C21)}$$

Where $\hat{\kappa} = \frac{C_1}{C_v}$ is thermal diffusion of soil, C_v [J m^{-3} K^{-1}] is soil heat capacity. C_v is given by Eq. (C22).

$$C_v = 2 \times 10^6 (1 - \theta_{sat}) + 4.2 \times 10^6 \times \theta \quad \text{(C22)}$$

Where θ_{sat} [m^3 m^{-3}] is saturated soil moisture.

Appendix D

Water balance

In the water balance equation (Eqs. 21 and 22), Leak is water infiltration from the upper to the deeper soil layer. Infiltration rate depends on soil texture and current soil moisture (Eq. D1) (Balsamo et al., 2009).

$$\text{Leak} = \rho_w \cdot \gamma \quad \text{(D1)}$$

Where γ [m s^{-1}] is the hydraulic conductivity (Eq. D2), ρ_w [kg H_2O m^{-3}] is liquid water density.

$$\gamma = \gamma_{sat} \frac{[(1 + \xi\psi^n)^{1-1/n} - \xi\psi^{n-1}]^2}{(1 + \xi\psi^n)^{(1-1/n)(\iota+2)}} \quad \text{(D2)}$$

GMDD
6, 4603–4663, 2013

Where γ_{sat} is saturated hydraulic conductivity (1.16×10^{-6} m s^{-1}), ξ, ι, n are parameters dependent on soil texture (Table A2), ψ is pressure head in meters that can be retrieved from Eq. (D3)

$$\theta_{[1;2]} = \theta_r + \frac{\theta_{sat} - \theta_r}{(1 + \xi\psi)^{1-1/n}} \quad \text{(D3)}$$

Where θ_r [m^3 m^{-3}] is the residual soil moisture, θ_{sat} [m^3 m^{-3}] is the saturated soil moisture dependent on soil texture (Table 3).

Supplementary material related to this article is available online at http://www.geosci-model-dev-discuss.net/6/4603/2013/gmdd-6-4603-2013-supplement.zip.

Acknowledgements. We would like to thank Aaron Boone for his help on getting climatic data from ALMIP project. We thank Utrecht University for financial support on this research.

References

Balsamo, G., Beljaars, A., Scipal, K., Viterbo, P., van den Hurk, B., Hirschi, M., and Betts, A.: A revised hydrology for the ECMWF model: Verification from field site to terrestrial water storage and impact in the Integrated Forecast System, J. Hydrometeorol., 10, 623–643, 2009. 4608, 4642

Baudena, M. and Provenzale, A.: Rainfall intermittency and vegetation feedbacks in drylands, Hydrol. Earth Syst. Sci., 12, 679–689, doi:10.5194/hess-12-679-2008, 2008. 4606, 4628, 4629

Baudena, M., D'Andrea, F., and Provenzale, A.: An idealized model for tree–grass coexistence in savannas: the role of life stage structure and fire disturbances, J. Ecol., 98, 74–80, 2010. 4605

GMDD
6, 4603–4663, 2013

Bonan, G.: Forests and climate change: forcings, feedbacks, and the climate benefits of forests, Science, 320, 1444–1449, 2008. 4604, 4605

Boone, A., Rosnay, P., Balsamo, G., Beljaars, A., Chopin, F., Decharme, B., Delire, C., Ducharne, A., Gascoin, S., Grippa, M., Jarlan, L., Kergoat, L., Mougin, E., Gusev, Y., Nasonova, O., Harris, P., Taylor, C., Norgaard, A., Sandholt, I., Ottlé, C., Poccard-Leclercq, I., Saux-Picart, S., and Xue, Y.: The AMMA land surface model Intercomparison Project (ALMIP), B. Am. Meteorol. Soc., 90, 1865–1880, 2009. 4607, 4620, 4658

Boussetta, S., Balsamo, G., Beljaars, A., Panareda, A.-A., Calvet, J.-C., Jacobs, C., Hurk, B., Viterbo, P., Lafont, S., Dutra, E., Jarlan, L., Balzarolo, M., Papale, D., and van der Werf, G.: Natural land carbon dioxide exchanges in the ECMWF Integrated Forecasting System: Implementation and offline validation, J. Geophys. Res.-Atmos., 118, 5923–5946, doi:10.1002/jgrd.50488, 2013. 4608, 4637

Calvet, J.: Investigating soil and atmospheric plant water stress using physiological and micrometeorological data, Agr. Forest Meteorol., 103, 229–247, 2000. 4606, 4607, 4608, 4609, 4612, 4613, 4616, 4617, 4631

Calvet, J., Rivalland, V., Picon-Cochard, C., and Guehl, J.: Modelling forest transpiration and CO_2 fluxes-response to soil moisture stress, Agr. Forest Meteorol., 124, 143–156, 2004. 4606, 4607, 4608, 4609, 4612, 4613, 4616, 4617, 4622, 4631

Cox, P.: Description of the "TRIFFID" dynamic global vegetation model, Hadley Centre Technical Note, 24, 1–16, 2001. 4607, 4611, 4613

Dekker, S. C., Bouten, W., and Verstraten, J. M.: Modelling forest transpiration from different perspectives, Hydrol. Process., 14, 251–260, 2000. 4637

Dekker, S., Rietkerk, M., and Bierkens, M.: Coupling microscale vegetation–soil water and macroscale vegetation–precipitation feedbacks in semiarid ecosystems, Global Change Biol., 13, 671–678, 2007. 4605

Dekker, S. C., de Boer, H. J., Brovkin, V., Fraedrich, K., Wassen, M. J., and Rietkerk, M.: Biogeophysical feedbacks trigger shifts in the modelled vegetation-atmosphere system at multiple scales, Biogeosciences, 7, 1237–1245, doi:10.5194/bg-7-1237-2010, 2010. 4604

Dekker, S., Vrugt, J., and Elkington, R.: Significant variation in vegetation characteristics and dynamics from ecohydrological optimality of net carbon profit, Ecohydrology, 5, 1–18, 2012. 4607

Dijkstra, H.: Vegetation Pattern Formation in a Semi-Arid Climate, Int. J. Bifurcat. Chaos, 21, 3497–3509, 2011. 4605

GMDD
6, 4603–4663, 2013

ECMWF: IFS DOCUMENTATION CY33R1. Part IV: Physical processes, Tech. rep., ECMWF, 2008. 4608, 4638
Entekhabi, D., Rodriguez-Iturbe, I., and Bras, R.: Variability in large-scale water balance with land surface-atmosphere interaction, J. Climate, 5, 798–813, 1992. 4605
Guan, K., Wood, E., and Caylor, K.: Multi-sensor derivation of regional vegetation fractional cover in Africa, Remote Sens. Environ., 124, 653–665, 2012. 4605, 4627
Higgins, S., Scheiter, S., and Sankaran, M.: The stability of African savannas: insights from the indirect estimation of the parameters of a dynamic model, Ecology, 91, 1682–1692, 2010. 4605
Hirota, M., Holmgren, M., Van Nes, E. H., and Scheffer, M.: Global resilience of tropical forest and savanna to critical transitions, Science, 334, 232–235, 2011. 4605
Holmgren, M. and Scheffer, M.: El Niño as a window of opportunity for the restoration of degraded arid ecosystems, Ecosystems, 4, 151–159, 2001. 4628
Jacobs, C., van den Hurk, B., and De Bruin, H.: Stomatal behaviour and photosynthetic rate of unstressed grapevines in semi-arid conditions, Agr. Forest Meteorol., 80, 111–134, 1996. 4612, 4634
Jarvis, P.: The interpretation of the variations in leaf water potential and stomatal conductance found in canopies in the field, Philos. Trans. Roy. Soc. London. B, 273, 593–610, 1976. 4608
Kéfi, S., Rietkerk, M., Alados, C., Pueyo, Y., Papanastasis, V., ElAich, A., and De Ruiter, P.: Spatial vegetation patterns and imminent desertification in Mediterranean arid ecosystems, Nature, 449, 213–217, 2007. 4605
Klausmeier, C.: Regular and irregular patterns in semiarid vegetation, Science, 284, 1826–1828, 1999. 4606
Konings, A. G., Dekker, S., Rietkerk, M., and Katul, G. G.: Drought sensitivity of patterned vegetation determined by rainfall-land surface feedbacks, J. Geophys. Res.-Biogeosci., 116, G04008, doi:10.1029/2011JG001748, 2011. 4606
Koster, R., Dirmeyer, P., Guo, Z., Bonan, G., Chan, E., Cox, P., Gordon, C., Kanae, S., Kowalczyk, E., Lawrence, D., Liu, P., Lu, C.-H., Malyshev, S., McAvaney, B., Mitchell, K., Mocko, D., Oki, T., Oleson, K., Pitman, A., Sud, Y. C., and Taylor, C. M., Verseghy, D., Vasic, R., Xue, Y., and Yamada, T.: Regions of strong coupling between soil moisture and precipitation, Science, 305, 1138–1140, 2004. 4605
Malhi, Y., Doughty, C., and Galbraith, D.: The allocation of ecosystem net primary productivity in tropical forests, Philos. Trans. Roy. Soc. B, 366, 3225–3245, 2011. 4613

GMDD
6, 4603–4663, 2013

Oleson, K., Dai, Y., Bonan, G., Bosilovich, M., Dickinson, R., Dirmeyer, P., Hoffman, F., Houser, P., Levis, S., Niu, G.-Y., Thornton, P., Vertenstein, M., Yang, Z.-L., and Zeng, X.: Technical description of the community land model (CLM), Tech. rep., NCAR Technical Note NCAR/TN-461+ STR, National Center for Atmospheric Research, Boulder, CO, 2004. 4608

Rietkerk, M., Boerlijst, M., van Langevelde, F., HilleRisLambers, R., van de Koppel, J., Kumar, L., Prins, H., and de Roos, A.: Self-organization of vegetation in arid ecosystems, The American Naturalist, 160, 524–530, 2002. 4605, 4606

Rietkerk, M., Brovkin, V., van Bodegom, P., Claussen, M., Dekker, S., Dijkstra, H., Goryachkin, S., Kabat, P., van Nes, E., Neutel, A., Nicholson, S. E., Nobre, C., Petoukhov, V.,Provenzale, A., Scheffer, M., and Seneviratne, S. I.: Local ecosystem feedbacks and critical transitions in the climate, Ecol. Complex., 8, 223–228, 2011. 4605

Rodriguez-Iturbe, I., D'odorico, P., Porporato, A., and Ridolfi, L.: On the spatial and temporal links between vegetation, climate, and soil moisture, Water Resour. Res., 35, 3709–3722, 1999. 4607

Sankaran, M., Hanan, N., Scholes, R., Ratnam, J., Augustine, D., Cade, B., Gignoux, J., Higgins, S., Le Roux, X., Ludwig, F., Ardo, J., Banyikwa, F., Bronn, A., Bucini, G., Caylor, K. K., Coughenour, M. B., Diouf, A., Ekaya, W., Feral, C. J., February, E. C., Frost, P. G. H., Hiernaux, P., Hrabar, H., Metzger, K. L., Prins, H. H. T., Ringrose, S., Sea, W., Tews, J., Worden, J., and Zambatis, N.: Determinants of woody cover in African savannas, Nature, 438, 846–849, 2005. 4605, 4627

Schymanski, S., Roderick, M., Sivapalan, M., Hutley, L., and Beringer, J.: A test of the optimality approach to modelling canopy properties and CO_2 uptake by natural vegetation, Plant. Cell Environ., 30, 1586–1598, 2007. 4607

Schymanski, S., Roderick, M., Sivapalan, M., Hutley, L., and Beringer, J.: A canopy-scale test of the optimal water-use hypothesis, Plant. Cell Environ., 31, 97–111, 2008. 4607

Schymanski, S. J., Kleidon, A., Stieglitz, M., and Narula, J.: Maximum entropy production allows a simple representation of heterogeneity in semiarid ecosystems, Philos. Trans. Roy. Soc. B, 365, 1449–1455, 2010. 4607, 4627

Seneviratne, S., Corti, T., Davin, E., Hirschi, M., Jaeger, E., Lehner, I., Orlowsky, B., and Teuling, A.: Investigating soil moisture–climate interactions in a changing climate: A review, Earth-Sci. Rev., 99, 125–161, 2010. 4605

Sitch, S., Smith, B., Prentice, I., Arneth, A., Bondeau, A., Cramer, W., Kaplan, J., Levis, S., Lucht, W., Sykes, M., Thonicke, K., and Venevsky, S.: Evaluation of ecosystem dynamics,

GMDD
6, 4603–4663, 2013

plant geography and terrestrial carbon cycling in the LPJ dynamic global vegetation model, Global Change Biol., 9, 161–185, 2003. 4607, 4610, 4611, 4613

Staver, A. C., Archibald, S., and Levin, S. A.: The global extent and determinants of savanna and forest as alternative biome states, Science, 334, 230–232, 2011. 4605

Teuling, A., Seneviratne, S., Stöckli, R., Reichstein, M., Moors, E., Ciais, P., Luyssaert, S., Van Den Hurk, B., Ammann, C., Bernhofer, C., Dellwik, E., Gianelle, D., Gielen, B., Grünwald, T., Klumpp, K., Montagnani, L., Moureaux, C., Sottocornola, M., and Wohlfahrt, G.: Contrasting response of European forest and grassland energy exchange to heatwaves, Nat. Geosci., 3, 722–727, 2010. 4605

van den Hurk, B., Viterbo, P., Beljaars, A., and Betts, A.: Offline validation of the ERA40 surface scheme, European Centre for Medium-Range Weather Forecasts, 2000. 4608

Zeng, N., Neelin, J. D., Lau, K. M., and Tucker, C. J.: Enhancement of interdecadal climate variability in the Sahel by vegetation interaction, Science, 286, 1537–1540, 1999. 4605

GMDD

6, 4603–4663, 2013

Table 1. Parameterization of vegetation with two strategies.

Parameters	Unit	Vegetation Type			Reference
		Grass	Woody		
			Defensive	Offensive	
$A_{max}(25\,^{\circ}C)$	$mg\,C\,m^{-2}\,s^{-1}$	0.6	0.49	0.49	Boussetta et al. (2013)
a_l	$kg\,C\,m^{-2}$	–	0.65	0.65	Cox (2001)
D_{max}	$g\,kg^{-1}$	–	0.1	0.1	Calvet et al. (2004)
D^N_{max}	$g\,kg^{-1}$	0.055	–	–	Calvet (2000)
D^X_{max}	$g\,kg^{-1}$	0.3	–	–	Calvet (2000)
f^*_0	–	–	0.606	0.46	Calvet (2000); Calvet et al. (2004)
f_0	–	0.95	–	–	Boussetta et al. (2013)
f_{wc}	$m^2\,m^{-2}$	0.5	0.1	0.6	Calvet (2000); Calvet et al. (2004)
$g^*_m(25\,^{\circ}C)$	$mm\,s^{-1}$	0.5	1.6	4.4	Calvet (2000); Calvet et al. (2004)
$\Gamma(25\,^{\circ}C)$	ppm	42	42	42	Boussetta et al. (2013)
ϵ^*_0	$10^{-3}\,mg\,C\,J^{-1}$	4.64	4.64	4.64	Boussetta et al. (2013)
τ_{leaf}	yr	1	1	1	–
τ_{stem}	yr	–	10	10	–
τ_{root}	yr	1	10	10	–
φ_{max}	$kg\,C\,m^{-2}$	1.0	10	10	–

GMDD
6, 4603–4663, 2013

Table 2. Variables in the maintext.

Symbols	Unit	Contents	Symbols	Unit	Contents
$a_{[v;b]}$	1	surface albedo of vegetation (bare ground)	C A	m^2	crown area
C_{veg}	kg C	biomass of vegetation	C_{leaf}	kg C	biomass of leaf
C_{root}	kg C	biomass of root	C_{stem}	kg C	biomass of stem
D	m	canopy structure factor	$E_{[v;b]}$	$kg\,H_2O\,m^{-2}\,s^{-1}$	evapotranspiration
f_c	1	leaf coverage	f_s	1	relative crown area
f_w, f_w^*	–	extractable water factor with(out) impact of root density	G P P	$kg\,C\,m^{-2}\,s^{-1}$	gross primary production
$G_{[v;b]}$	$W\,m^{-2}$	soil heat flux	g_a	$m\,s^{-1}$	aerodynamic conductance
g_m	$m\,s^{-1}$	mesophyll conductance	$g_{s,[v;b]}$	$m\,s^{-1}$	surface conductance
$H_{[v;b]}$	$W\,m^{-2}$	sensible heat flux	$lE_{[v;b]}$	$W\,m^{-2}$	latent heat flux
LIT	$kg\,C\,m^{-2}\,s^{-1}$	litter production	LAI	1	leaf area index
$Leak_{[1;2]}$	$kg\,H_2O\,m^{-2}\,s^{-1}$	water leakage	N P P	$kg\,C\,m^{-2}\,s^{-1}$	net primary production
P_s	Pa	surface pressure	P	$kg\,H_2O\,m^{-2}\,s^{-1}$	precipitation rate
q_a	Pa	actual vapor pressure	q_s	Pa	saturated vapor pressure
R_d	$kg\,C\,m^{-2}\,s^{-1}$	dark respiration	R_{WU}	1	relative water use
R_{space}	1	relative space of bare soil	$R_{n,[v;b]}$	$W\,m^{-2}$	net radiation
R_{lwd}	$W\,m^{-2}$	downward long wave radiation	R_{swd}	$W\,m^{-2}$	downward short wave radiation
SH	$kg\,kg^{-1}$	specific humidity at 2 m	t	s	simulation time step
T_a	K	air temperature at 2 m	$T_{s,[v;b]}$	K	surface temperature
$T_{[1;2]}$	K	temperature of soil layer 1 and 2	u_n	$m\,s^{-1}$	u direction wind speed
v_n	$m\,s^{-1}$	v direction wind speed	$W_{[1;2]}$	$kg\,H_2O$	total water stored in soil layers
α	1	shoot-total biomass ratio	$\theta_{[1;2]}$	$m^3H_2O\,m^{-3}$	soil moisture
ρ_a	$kg\,m^{-3}$	mean air density at constant pressure	φ	1	root density

GMDD
6, 4603–4663, 2013

Table 3. Constants in the maintext.

Symbols	Value	Contents	Symbols	Value	Contents
a	1.6	diffusivity constants of H_2O and CO_2	a_b	0.4	albedo of bare ground
a_{max}	0.4	maximum albedo of vegetation	a_{min}	0.1	minimum albedo of vegetation
CA_{ref}	$15\,m^2$	maximum crown area	c_p	$1013\,J\,kg^{-1}\,K^{-1}$	specific heat capacity of air
$g_{s,max}$	$0.2\,m\,s^{-1}$	maximum bare ground conductance	LAI_{ref}	6	referred LAI
l	$2.45 \times 10^6\,J\,kg^{-1}$	latent heat of vaporization	SLA	$20\,m^2\,kg^{-1}$	specific leaf area
$z_{[1;2]}$	0.02; 0.48 m	depth of layer 1 (2)	ϵ	0.96	surface emissivity
θ_{pwp}	0.151	soil moisture at wilting point	θ_{cap}	0.346	soil moisture at field capacity
θ_r	0.01	residual soil moisture	θ_{sat}	0.439	saturated soil moisture
σ	$5.67 \times 10^{-8}\,W\,m^{-2}\,K^{-4}$	Stefan-Boltzmann constant			

GMDD
6, 4603–4663, 2013

Table A1. Variables appeared in Appendix.

Symbols	Unit	Variables
A_{max}	kg C m^{-2} s^{-1}	maximum carbon assimilation rate
A_m	kg C m^{-2} s^{-1}	maximum carbon assimilation rate limited by CO_2
A_n	kg C m^{-2} s^{-1}	carbon assimilation rate effected by radiation
C_H	1	transfer coefficients to heat
C_M	1	transfer coefficients to momentum
C_Q	1	transfer coefficients to humidity
C_v	J m^{-3} K^{-1}	thermal capacity of soil
c_i	ppm	intercellular CO_2 concentration
c_p	J kg^{-1} K^{-1}	specific heat capacity of moist air
D^*_{max}	kg kg^{-1}	maximum vpD without water stress
f	1	coupling factor that controls opening of stomata
f_0^N	1	f_0 corresponding to g^*_m
Γ	ppm	compensation concentration of CO_2
γ	m s^{-1}	soil hydraulic conductivity
g_m^N	mm s^{-1}	mesophyll conductance corresponding to D^X_{max}
g_m^X	mm s^{-1}	mesophyll conductance corresponding to D^N_{max}
g_{sc}	m s^{-1}	stomata conductance of CO_2
$\hat{h}$	m m^{-1}	relative height of vegetation
I_a	W m^{-2}	photo active radiation at top of stomata
L	m	Obukhov length
J_M	J m^{-2}	momentum flux
J_q	W m^{-2}	latent heat flux
J_s	W m^{-2}	sensible heat flux
K_{df}	1	extinction coefficients of diffuse light
K_{dr}	1	extinction coefficients of direct light
P A R	W m^{-2}	photo active radiation at top of canopy
Q_{0v}	K	virtual temperature flux in the surface layer
q_*	m s^{-2}	humidity turbulence
R_d	kg C m^{-2} s^{-1}	dark respiration rate
s_*	m s^{-2}	heat turbulence
U_n	m s^{-1}	horizontal wind speed
u_*	m s^{-1}	wind speed
vpD	kg kg^{-1}	vapor pressure deficit
ϵ^*	kg J^{-1}	quantum use efficiency
ζ	1	stability factor of the surface layer
$\hat{\kappa}$	m^2 s^{-1}	thermal diffusivity of soil
ψ	m	pressure head

GMDD
6, 4603–4663, 2013

Table A2. Constants used in Appendix.

Symbols	Unit	Description	Value
a	–	constant used in Monin-Obukhov similiarity theory	1
a_1	–	factor in relation of $g_m(25\,^{\circ}C)$ and D_{max}	2.381
b	–	constant used in Monin-Obukhov similiarity theory	0.667
b_l	1	foliage scattering coefficient	0.944
b_1	–	factor in relation of $g_m(25\,^{\circ}C)$ and D_{max}	0.6103
C_1	$W\,m^{-1}\,K^{-1}$	thermal conductivity of soil	0.2
c	–	constant used in Monin-Obukhov similiarity theory	5
c_a	ppm	CO_2 concentration in the air	388
$c_{p_{dry}}$	$J\,kg^{-1}\,K^{-1}$	specific heat capacity of dry air	1013
$c_{p_{vap}}$	$J\,kg^{-1}\,K^{-1}$	specific heat capacity of water vapor	2080
d	–	constant used in Monin-Obukhov similiarity theory	0.35
e	1	ratio of molecular weight of water to dry air	0.622
G_l	1	leaf distribution parameter	0.5
g	$m\,s^{-2}$	acceleration due to gravity	9.8
n	–	soil texture parameter	1.28
Q_{Am}, Q_g, Q_Γ	–	exponential factor in Q_{10} curve	2
$T_{1,Am}$	$^{\circ}C$	reference temperature for A_{max} in Q_{10} curve	8
$T_{2,Am}$	$^{\circ}C$	reference temperature for A_{max} in Q_{10} curve	38
$T_{1,g}$	$^{\circ}C$	reference temperature for g_m in Q_{10} curve	36
$T_{2,g}$	$^{\circ}C$	reference temperature for g_m in Q_{10} curve	5

GMDD
6, 4603–4663, 2013

Table A2. Continued.

Symbols	Unit	Description	Value
z_n	m	height of measurement	2
z_{0H}	m	height of heat measurement	0.02
z_{0M}	m	height of wind measurement	0.2
z_{0Q}	m	height of humidity measurement	0.02
γ_{sat}	$m\,s^{-1}$	saturated hydraulic conductivity	1.16×10^{-6}
δ	1	ration of diffuse to total downward shortwave radiation at the top of the layer	0.2
ι	–	soil texture parameter	−2.342
κ	–	Von Karman's constant	0.41
μ_s	°	solar zenith angle	90
ξ	m^{-1}	soil texture parameter	3.14
ρ_w	$kg\,m^{-3}$	liquid water density	10^3
ω	1	scattering albedo	0.2

GMDD
6, 4603–4663, 2013

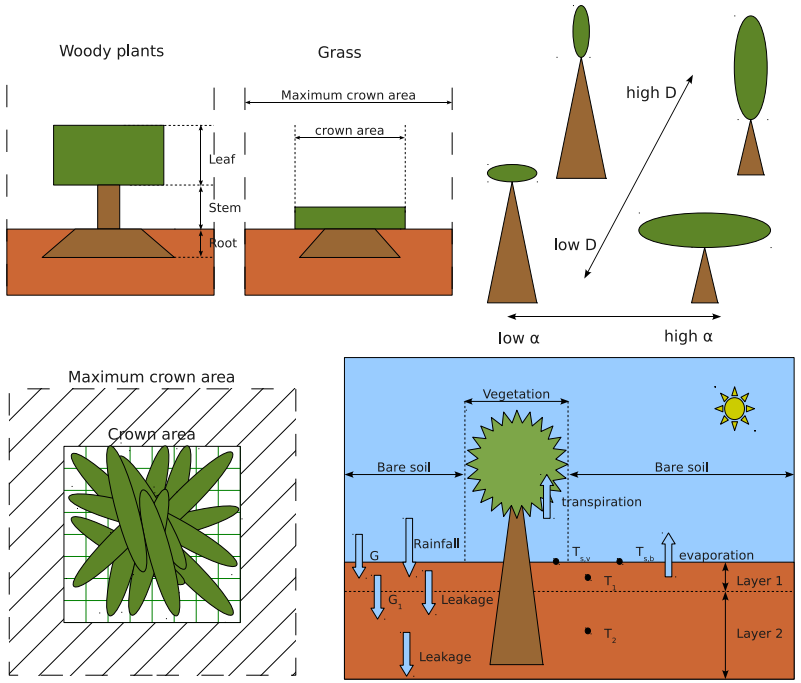

Fig. 1. Conceptual plot of vegetation structures and carbon-water-energy coupled model. Top left panel shows the composition of biomass for grass and woody plants (Eq. 4). Plant biomass is divided into above ground (leaves and stems) and below ground (roots) biomass. The top right panel illustrates the control of the vegetation structure by the parameters α (fraction of above ground biomass over total biomass, Eq. 5) and D (canopy shape parameter, Eq. 8). A high value for D represents a vertically oriented canopy. In the bottom left panel, the largest rectangle is the referenced crown area CA_{ref}, while the smaller rectangle denotes the real crown area CA. Within the CA, a fraction is covered by leafs, which depends on LAI (Eq. 9). The bottom right panel shows the tiling method (Eq. 13), the two-layer soil scheme (Eq. 21 and 22) and the representation of water balances and soil heat fluxes.

GMDD
6, 4603–4663, 2013

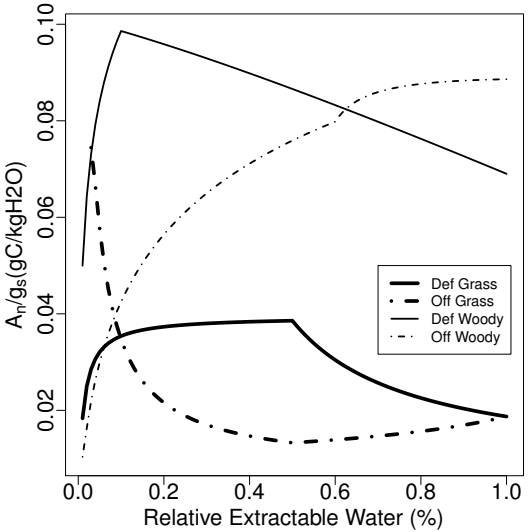

Fig. 2. Intrinsic W U E as a function of extractable water. Extractable water (f_w) is defined as Eq. (12). Solid and dot-dashed lines represent defensive and offensive strategies respectively. Thick and thin lines represents grass and woody plants respectively. vpD = 12 g kg^{-1}, L A I = 1, R_{swd} = 800 W m^{-2}, c_a = 380 ppm and T_s = 25 °C.

GMDD
6, 4603–4663, 2013

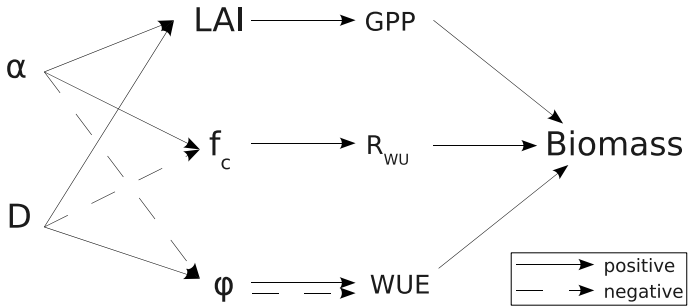

Fig. 3. Impacts of α and D on vegetation biomass via six variables. Solid and dashed lines represent positive and negative impact respectively. R_{WU} is the relative water use, defined in Eq. (24). φ is root density. WUE is water use efficiency defined in Eq. (23).

GMDD
6, 4603–4663, 2013

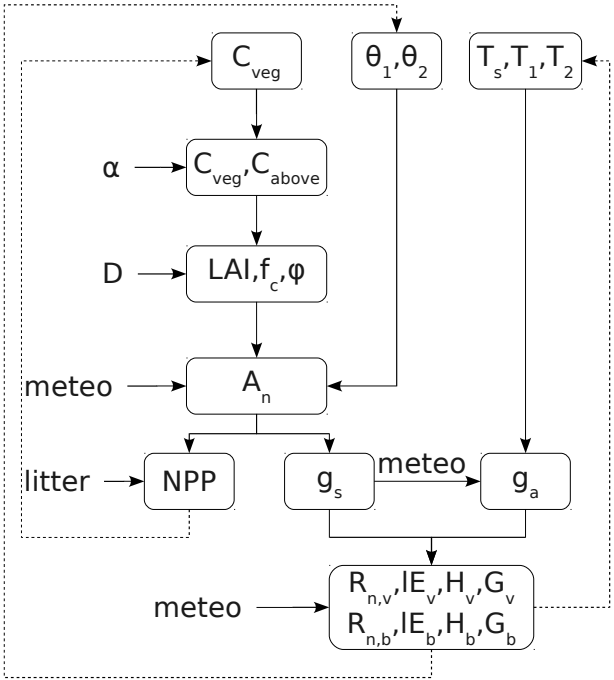

Fig. 4. Flow diagram of the model. Dashed arrows imply time step updates. For symbols see text.

GMDD
6, 4603–4663, 2013

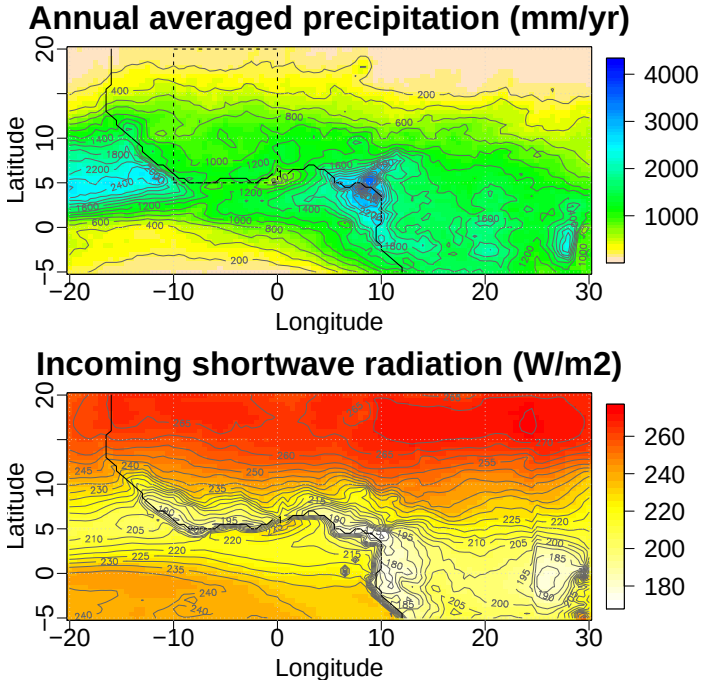

Fig. 5. Annual mean preicipitation and incoming shortwave radiation distribution in West Africa. Region marked is the study domain, ranging between 20° W to 30° E and from 5° S to 20° N in West Africa. Data is from the ALMIP forcing data set Boone et al. (2009).

GMDD
6, 4603–4663, 2013

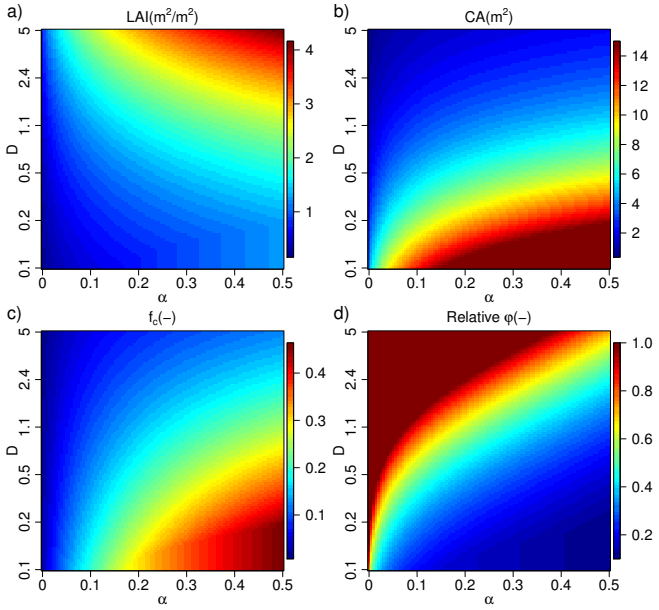

Fig. 6. Patterns of woody vegetation for different combinations of α and D. α is varied from 0 to 0.5. D is set from 0.1 to 5. Total biomass is 30 kg C per pixel of 15 m^2. Panel **(a)**: LAI; **(b)**: f_c; **(c)**: C A; **(d)**: relative φ. Relative φ is defined as φ/φ_{max}. When $\varphi > \varphi_{max}$, value of relative φ is set to one.

GMDD
6, 4603–4663, 2013

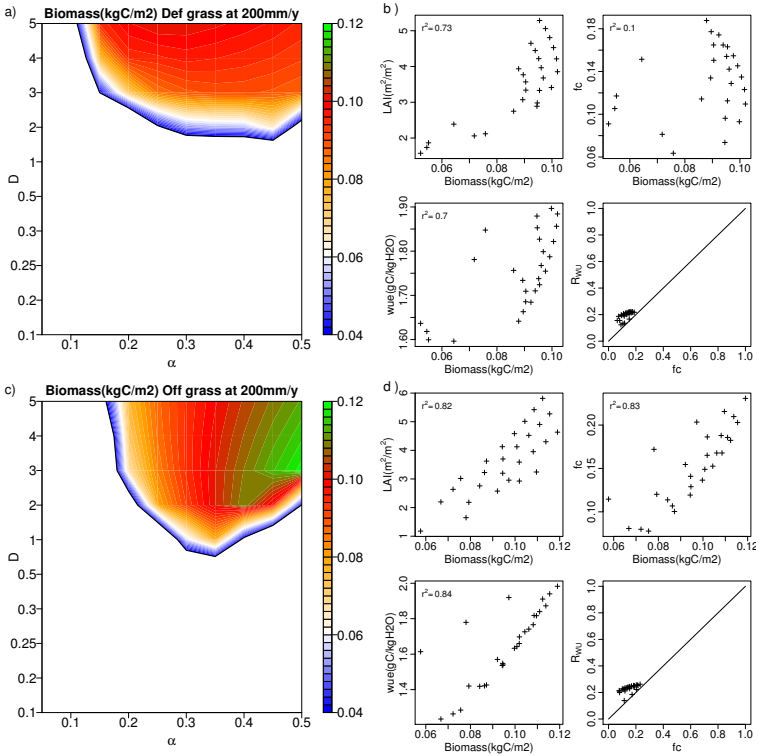

Fig. 7. Sensitivity analysis of equilibrium biomass to vegetation structure: A. Panels **(a)** and **(c)** present six-year averaged total biomass that changes with different vegetation structures of two strategies. Patterns represent survival structures under the specified regime. Panels **(b)** and **(d)** display several variables (LAI, f_c and W U E) as a function of biomass and a comparison between f_c and R_{WU}. Soild lines in Panels **(b)** and **(d)** are one-one line. Panels **(a)** and **(b)** are for defensive grass case under 200 mm yr^{-1}. Panels **(c)** and **(d)** are for offensive grass case.

GMDD
6, 4603–4663, 2013

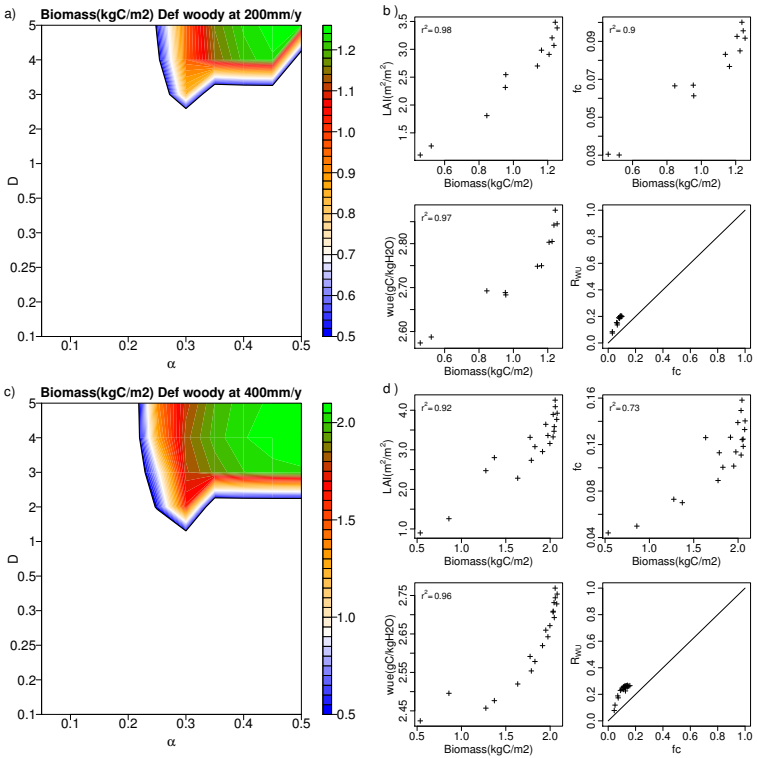

Fig. 8. Sensitivity analysis of equilibrium biomass to vegetation structure: B. As Fig. 7, defensive woody vegetation case for 200 mm yr^{-1} (panels **a** and **b**) and 400 mm yr^{-1} (**c** and **d**).

GMDD
6, 4603–4663, 2013

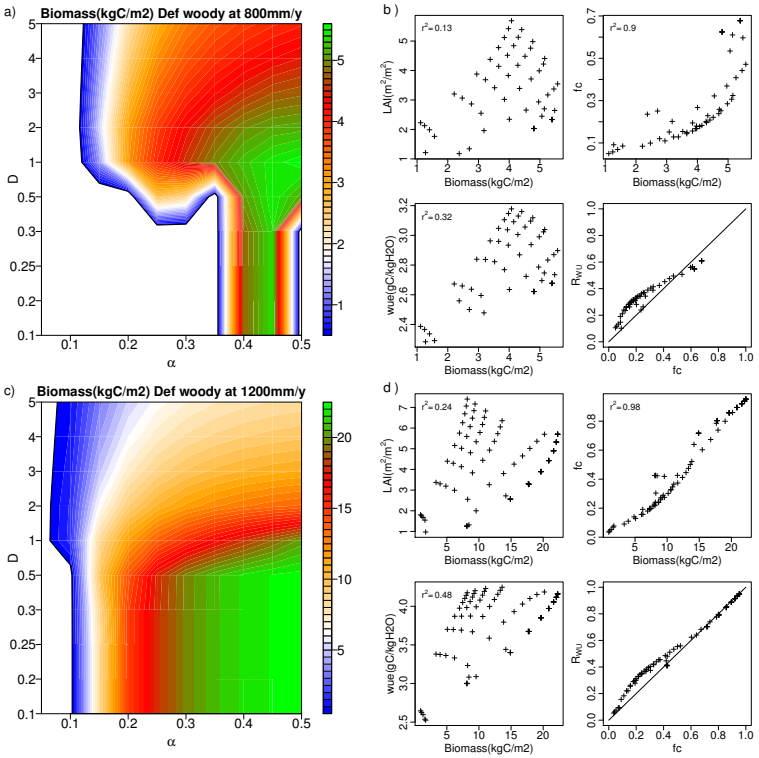

Fig. 9. Sensitivity analysis of equilibrium biomass to vegetation structure: C. As Fig. 8 for 800 mm yr^{-1} (panels **a** and **b**) and 1200 mm yr^{-1} (**c** and **d**).

GMDD
6, 4603–4663, 2013

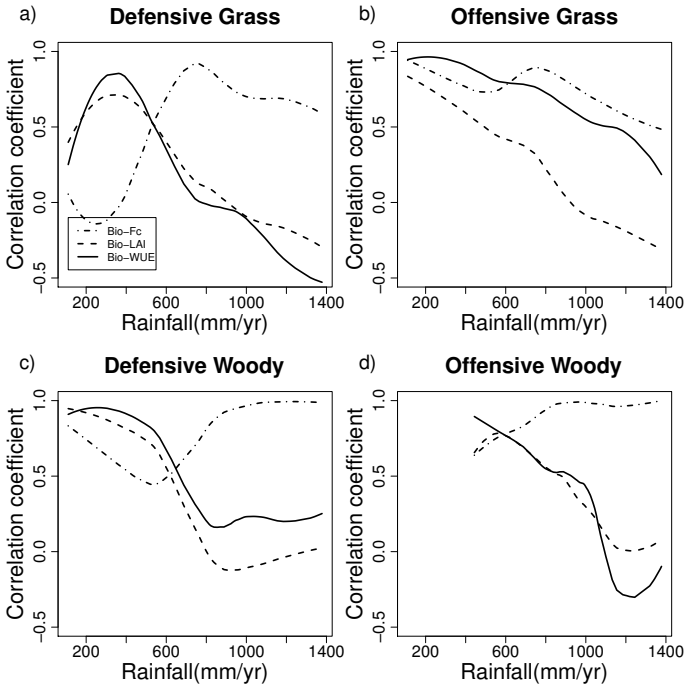

Fig. 10. Dominant factor change with precipitation. Correlation coefficients between averaged biomass and three parameters as a function of mean annual precipitation. Panels **(a)**, **(b)**, **(c)** and **(d)** represent defensive grass, offensive grass, defensive woody and offensive woody respectively. Dot-dashed, dashed and solid lines are for correlation between biomass and f_c, LAI and W U E, respectively.

GMDD
6, 4603–4663, 2013